Electron Spin Resonance
in Biophysical Chemistry

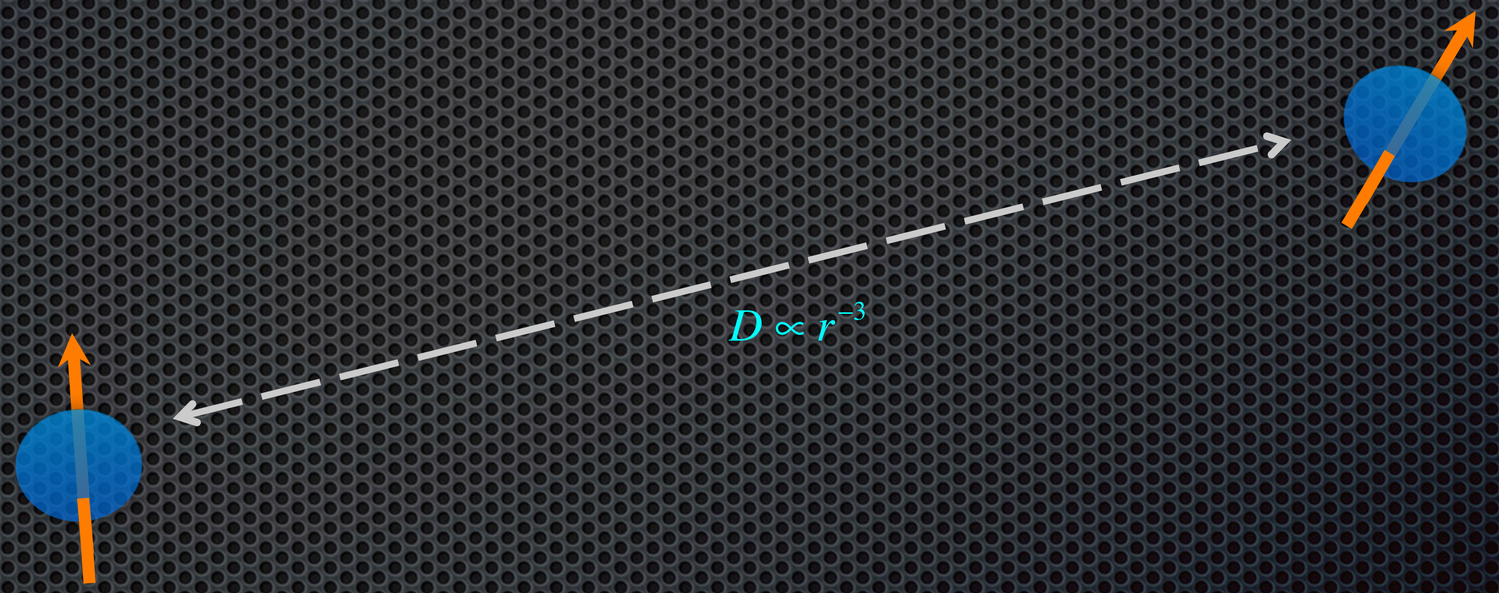

Basic Principles

- Spin angular momentum vector $\hat{S}\hbar$, $\hat{I}\hbar$, $\hbar = \frac{h}{2\pi}$

  (Intrinsic Spin ; Purely QM !!)

- Magnetic Moment

$$\vec{\mu} = -\gamma \hbar \hat{S} = -g \beta \hat{S}$$

- γ: Gyromagnetic ratio
- β: Bohr magneton $= \frac{e\hbar}{2m}$ (β_e, β_N, β_B)
  - charge: e
  - mass: proton or ele.
- g: g factor (Dimensionless, intrinsic)

phys. meaning ↓

$$\rightarrow |\gamma| = \frac{g\beta}{\hbar} = \frac{ge}{2m} = \frac{\text{mag. moment } \mu}{\text{Int. Spin ang. momentum. } \hbar\hat{s}}$$

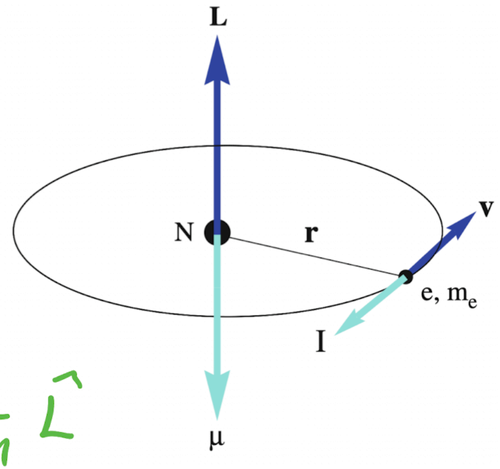

Fig. 1.1 Classical model illustrating relationship between angular momentum $L = m_e \cdot v \cdot r$ of electron, e, moving around a nucleus N and magnetic moment μ.

$$\mu = I \cdot A = \cdots = -\frac{e}{2m}\hat{L}$$

TABLE 28.1 Parameters for Spin-Active Nuclei

Nucleus	Isotopic Abundance (%)	Spin	Nuclear g Factor g_N	Magnetogyric Ratio $\gamma/10^7$ (rad $T^{-1} s^{-1}$)
^1H	99.985	1/2	5.5854	26.75
^{13}C	1.108	1/2	1.4042	6.73
^{31}P	100	1/2	2.2610	10.84
^2H	0.015	1	0.8574	4.11
^{14}N	99.63	1	0.4036	1.93

$$\frac{m_p}{m_e} = \frac{1.67 \times 10^{-24}\ g}{9.1 \times 10^{-28}\ g} \sim 1835$$

$g_e = 2.0023$, $g_N = 5.5854$

$\beta_e = 9.274 \times 10^{-24}$ J/T

$\beta_N = 5.0504 \times 10^{-27}$ J/T

$\therefore \frac{\mu_e}{\mu_N} \sim 658 \Rightarrow \mu_e \cong 658\,\mu_N$

↪ better sensitivity per spin.

- $\hat{S}_z |\alpha\rangle = +\frac{1}{2} |\alpha\rangle$

  $\hat{S}_z |\beta\rangle = -\frac{1}{2} |\beta\rangle$

- m_s : Electron spin Q.N.

  e.g. $S = \frac{1}{2} \Rightarrow m_s = \pm 1/2$

- WHEN WE APPLY A STEADY MAGNETIC FIELD B ON A SPIN, THE INTERACTION BETWEEN B AND μ CAN BE EXPRESSED IN TERMS OF HAMILTONIAN:

$$\hat{\mathcal{H}} = -\vec{\mu} \cdot \vec{B}_0$$

→ If we only consider B (or H) in z direction,

$$\langle \hat{\mathcal{H}} \rangle = E = \gamma \hbar B_0 m_s = g \beta B_0 m_s$$

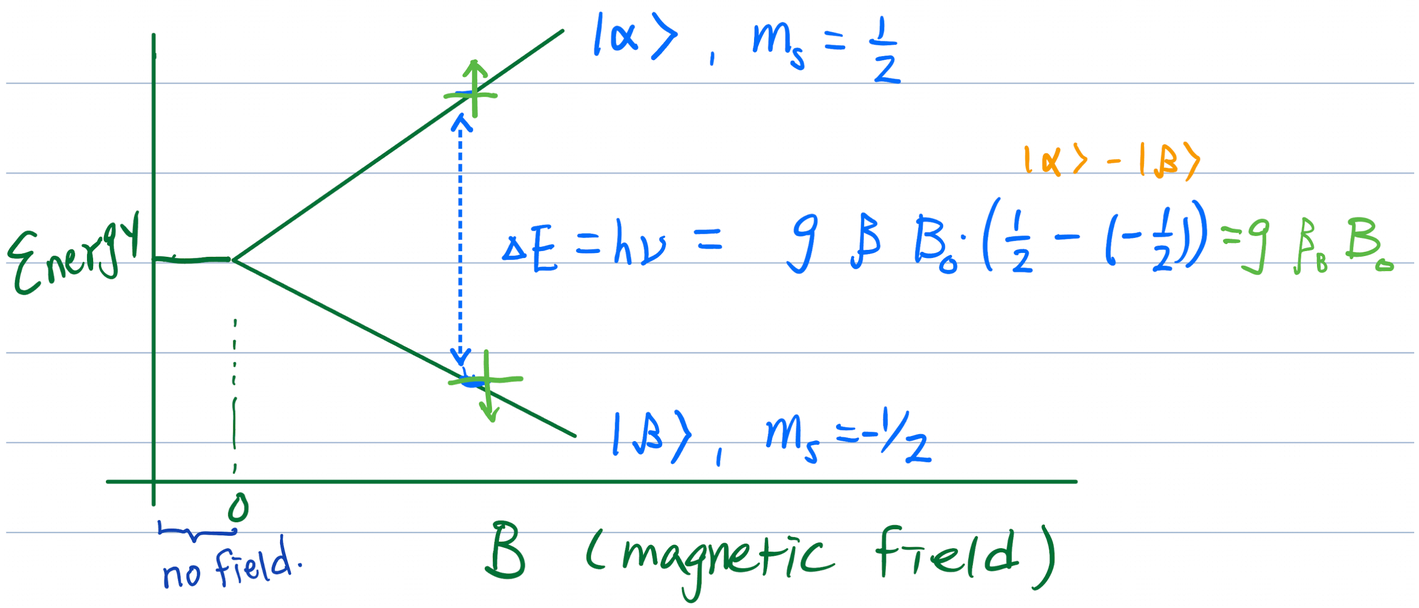

(Zeeman effect)

→ In order to induce transition between $|\alpha\rangle$ and $|\beta\rangle$, we apply an oscillating electromagnetic field to provide energy of frequency ν to satisfy the resonance condition,

→ In terms of angular frequency ω [rs^{-1}]

$\because \frac{\omega}{2\pi} = \nu \quad \Rightarrow \quad \omega = \gamma B_0 \propto B_0$

$\hbar$

Larmor Frequency.

[s^{-1}]. e.g. $\frac{1}{\mu s} \rightarrow MHz$.

Note:

$2\pi\nu = \frac{g\beta}{\hbar} B_0$

$h\nu = g\beta B_0$

- To induce the transition: tune ω as B_0 Fixed. or vice versa.

→ modern NMR: radio freq. pulse techniques.

e.g. $^1H \Rightarrow 500\ MHz \rightarrow 12$ Tesla.

e.g. $\frac{B_0(NMR)}{B_0(EPR)} \sim \frac{\omega_N}{\gamma_N} \cdot \frac{\gamma_e}{\omega_e} = 658 \cdot \frac{0.5\,GHz}{9\,GHz} \sim 37 \quad \therefore B_0(EPR) \sim \frac{12}{37} = 0.33$ Tesla

e.g. Why not using NMR source (e.g. 500 MHz) to pump e^- spin ?

ESR and NMR are very different methods!

	electron	***proton***	***ratio***
Rest mass	m_e =9.1094×10^{-28} g	m_p =1.6726×10^{-24} g	5.446×10^{-4}
Charge	e=-4.80286×10^{-10}ESU	e=4.80286×10^{-10}ESU	-1
Spin angular momentum	$h/4\pi$	$h/4\pi$	1
Magnetic dipole moment	$\mu_S = g_e \beta_e \boldsymbol{S}$ g_e= 2.002322 $\beta_e = eh/4\pi m_e c$ = 9.274×10^{-24} J/T	$\mu_N = g_N \beta_N \boldsymbol{S}$ g_N= 5.5856 $\beta_N = eh/4\pi m_N c$ = 5.0504×10^{-27} J/T	658

$\Rightarrow \mu_e \cong 658\, \mu_N$

↪ better sensitivity per spin.

- ***Frequency:*** Factor 1000 larger in EPR ! *(GHz instead of MHz)*
- ***Relaxation Times:*** Factor 1000 000 smaller in EPR ! *(ns instead of ms)* = much higher technical requirements, but unique sensitivity to molecular motion
- ***Sensitivity :*** Factor 1 000 000 better than in NMR !! *(1nM instead of 1mM)* *An ideal case, though*

1000 (freq)x 658 ~ 10^6

The Basic ESR Experiment (conventional ESR)

- ESR is done from 1 to 300+GHz, up to 2000+ GHz
  - Machines are classified according to their **source frequency** :
    L (1.5), **S** (3.0), **C** (6.0), X (9), **Ku** (17), **K** (23), **Q** (36), **V** (50), **W** (95), **D**(140), **G**(180)
- Use **microwave transmission lines**
- Do spectroscopy with a few microwatts to a few milliwatts of power
- Solid state [**Gunn diode** or DRO] or tube [**klystron**] sources
- **Temperatures** from 4K (heme and non-heme iron) to 310K+ (in vivo/vitro)
- **Sensitivity** : Increases as $(\text{frequency})^2$, but limited by sample size, field homogeneity and component construction problems.
- Practically (at X-band): detect 10^{10} spins, a detectable concentration of ~10^{-9}M. (under the condition of 100 μL)

Band name	Typical frequency ν in GHz	Wavelength λ in mm	Energy $h\nu$ in reciprocal cm	Resonance field B at g = 2 in tesla
L-band	1	300	0.033	0.036
S-band	3	100	0.10	0.11
C-band	6	50	0.20	0.21
X-band	10	30	0.33	0.36
P-band	15	20	0.50	0.54
K-band	24	12.5	0.80	0.86
Q-band	35	8.6	1.2	1.25
U-band	50	6.0	1.7	1.78
V-band	65	4.6	2.2	2.32
E-band	75	4.0	2.5	2.68
W-band	90	3.3	3.0	3.22
F-band	110	2.7	3.7	3.93
D-band	130	2.3	4.3	4.64
G-band	180	1.67	6.0	6.43
J-band	270	1.11	9.0	9.64
No name	600	0.50	20	21.4
No name	1000	0.30	33	35.7

Sensitivity

$$\text{Net Absorption} \propto N_- - N_+$$

The ratio of populations at equilibrium is given by the Boltzmann distribution

$$\frac{N_+}{N_-} = e^{-\Delta E/k_B T} = e^{-g\mu_B B/k_B T}$$

$$\frac{N_+}{N_-} \approx 1 - \frac{g\mu_B B}{k_B T} \longrightarrow N_- - N_+ = N_-\left[1 - \left(1 - \frac{g\mu_B B}{k_B T}\right)\right] = \frac{N g\,\mu_B B}{2\,k_B T}$$

- Net absorption increases with decreasing T, and with increasing magnetic field strength. (ΔN determines the bet absorption.)
- Higher frequency uses smaller waveguides, thus smaller sample volume, canceling the advantages (possibly).
- X-band can detect 10^{12} spins (10^{-12} moles) at room T. (on the order of 0.1 G wide)

The fractional excess population is:

$$\frac{n_2}{n_1} = e^{-\Delta E / kT}, \quad \Delta E = g\beta B_0$$

$$\frac{\Delta n}{n} = \frac{n_1 - n_2}{n_1 + n_2} = \frac{1 - e^{-\Delta E / kT}}{1 + e^{-\Delta E / kT}}$$

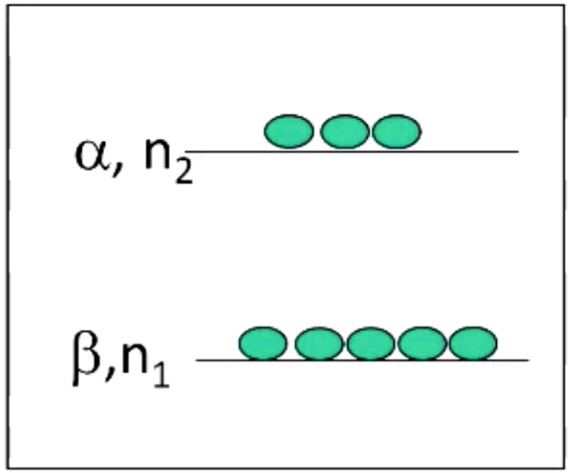

$$M_0 \propto n_1 - n_2$$

B_0(T)

	Δn/n	300 K	77 K	1.5 K
e	9.5 GHz	0.0008	0.002	0.1508
~0.3 ^{1}H	14.5 MHz	0.0012x10^{-3}	0.00395x10^{-3}	0.2320 x10^{-3}
~3	95 GHz	0.0076	0.0253	0.9087
	145 MHz	0.0116x10^{-3}	0.0387x10^{-3}	2.3196x10^{-3}
~9.6	263 GHz	0.0210	0.0700	0.9996
	400 MHz	0.0320x10^{-3}	0.1066 x10^{-3}	6.3989x10^{-3}

• In an Equilibrium Spin System $N = N_\alpha + N_\beta$

→ Boltzmann Law:

$$\frac{N_\beta}{N_\alpha} = \exp(-\Delta E / kT)$$

for $\Delta E = h\nu = g\beta B_0$

$$\Rightarrow \frac{N_\beta}{N_\alpha} \approx 1 - \frac{\Delta E}{kT}$$

$$\therefore N_\alpha - N_\beta = N_\alpha \left[1 - \left(1 - \frac{\Delta E}{kT}\right)\right] = \frac{N_\alpha \Delta E}{kT}$$

$$\approx \frac{N}{2} \frac{\Delta E}{kT} \propto \frac{h\nu_0}{T} \text{ or } \frac{\beta B_0}{T}$$

① $T \downarrow$ or $\nu_0 \uparrow$ or $B_0 \uparrow \Rightarrow \Delta N \uparrow$

② $\nu_e \sim 658\, \nu_H$ (at the same B_0)

EXAMPLE PROBLEM 28.1

a. Calculate the two possible energies of the ^1H nuclear spin in a uniform magnetic field of 5.50 T.

b. Calculate the energy ΔE absorbed in making a transition from the α to the β state. If a transition is made between these levels by the absorption of electromagnetic radiation, what region of the spectrum is used?

c. Calculate the relative populations of these two states in equilibrium at 300. K.

Solution

a. The two energies are given by

$$E = \pm\frac{1}{2} g_N \beta_N B_0$$

$$= \pm\frac{1}{2} \times 5.5854 \times 5.051 \times 10^{-27}\ \text{J/T} \times 5.50\ \text{T}$$

$$= \pm 7.76 \times 10^{-26}\ \text{J}$$

b. The energy difference is given by

$$\Delta E = 2(7.76 \times 10^{-26}\ \text{J})$$

$$= 1.55 \times 10^{-25}\ \text{J} \qquad \sim 10^{-3}\ \text{cm}^{-1}$$

$$\nu = \frac{\Delta E}{h} = \frac{1.55 \times 10^{-25}}{6.626 \times 10^{-34}} = 2.34 \times 10^{8}\ \text{s}^{-1}$$

This is in the range of frequencies called radio frequencies.

c. The relative populations of the two states are given by

$$\frac{n_\beta}{n_\alpha} = \exp\left(-\frac{E_\beta - E_\alpha}{k_B T}\right) = \exp\left(\frac{-2 \times 7.76 \times 10^{-26}\ \text{J}}{1.381 \times 10^{-23}\ \text{J K}^{-1} \times 300.\ \text{K}}\right) = 0.999963$$

$$\frac{n_\alpha - n_\beta}{\frac{1}{2}(n_\beta + n_\alpha)} \approx \frac{(1 - 0.999963)\, n_\alpha}{n_\alpha} = 3.7 \times 10^{-5} \qquad \text{or } \frac{n_\alpha - n_\beta}{n_\alpha + n_\beta} \approx \frac{n_\alpha (1 - 0.999963)}{2 n_\alpha}$$

$$= 1.85 \times 10^{-5}$$

From this result, we see that the populations of the two states are the same to within a few parts per million. Note that observing the appropriate rules for significant figures, we would obtain a ratio of 1.00.

$\Rightarrow E_\beta - E_\alpha \ll kT$, but $n_\alpha \approx n_\beta$

$\Rightarrow$ upward transition rate $\approx$ downward.

Structure and Stability of Nitroxides

Nitroxides are compounds containing the $>N^{\bullet}-O$ group which has an unpaired electron. The unpaired electron is located in a $2p_{\pi}$ (π^*) orbital of the nitrogen and the oxygen atom. Since there is also an N-O σ-bond and two electrons that fill a π-bonding orbital between these atoms, the effective N-O bond order is 1.5 (two center- three electron- bonding, 2c-3e). The structure of this group can be considered as a superposition of two mesomeric structures [34]

Scheme 2.1 Mesomeric formula of the nitroxide group.

The contributions of both structures to the ground state may be different, depending on the polarity of the medium and conjugation within the molecule. In apolar solvents both structures have the same weight while polar solvents will favor the charged mesomeric structure, leading to a higher charge density on the nitrogen (which can be observed as increased nitrogen hyperfine splitting in EPR spectra). The electronic structure is influenced in a similar way by π-complex formation with aromatic rings. Depending on the structure, the spin density on oxygen is ρ_o=0.58-0.72 and on nitrogen it is ρ_N=0.42-0.28 [35].The dipole moment of the N-O bond is 2.7 D and the distance is 1.26-1.29 A. The 2c-3e N-O bond has an energy of 419 kJ/mol, midway between the energy of an N-O single bond (230 kJ/mol) and N=O double bond (600 kJ/mol) [36]. As a result of the electron delocalization, nitroxides are relatively stable molecules. The energy gain from delocalization has been calculated as 126 kJ/mol [37].

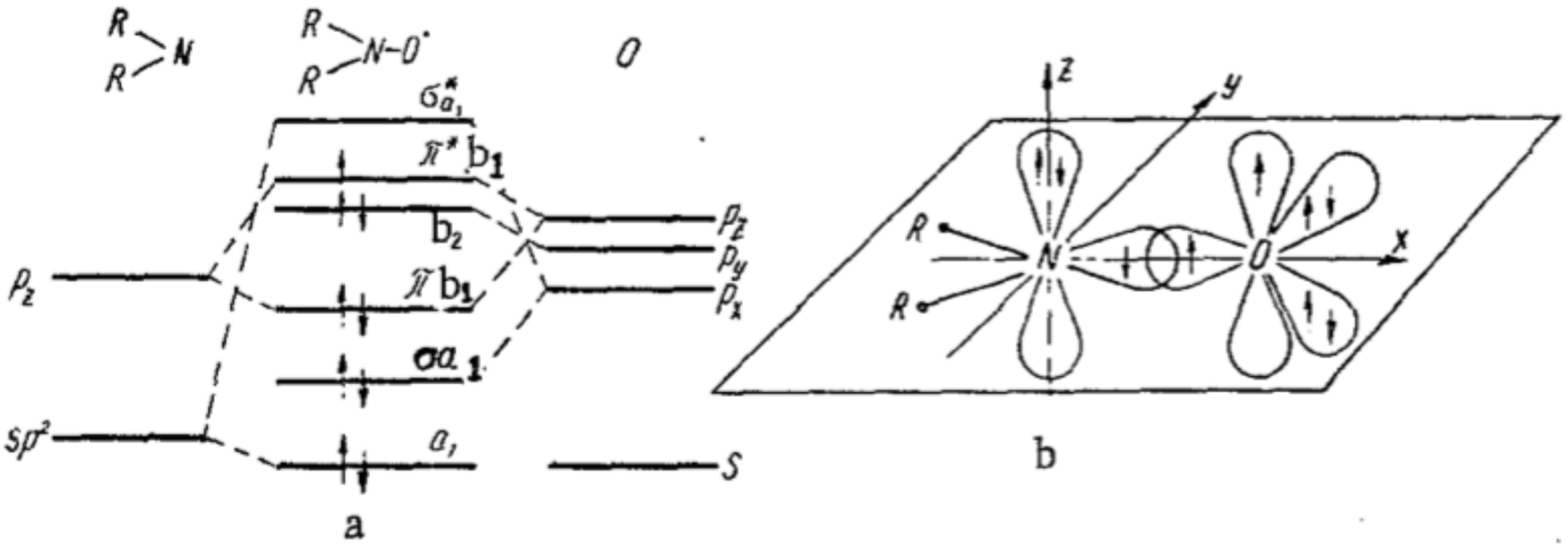

Fig. 2. Schematic representation of the energy levels (a) and electronic configuration (b) of the $\rangle$N—O· fragment of a free nitroxide radical [15].

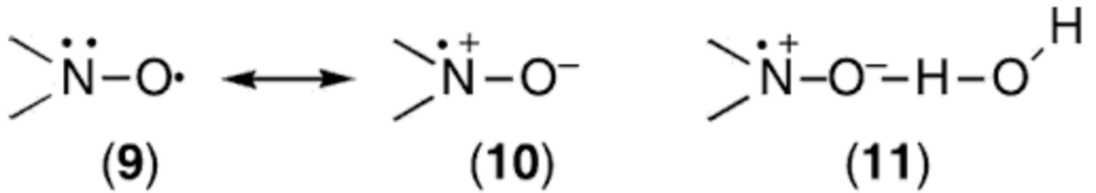

(9) (10) (11)

derived nitroxides. The nitrogen hfs constants of nitroxides also exhibit a marked solvent dependence, because nitroxides exist as the result of the two mesomeric forms **9** and **10**; in apolar solvents, the two forms have the same weight and thus 50% of the spin density resides on the nitrogen atom and the remaining 50% on the oxygen. In contrast, polar solvents will favor form **10** with respect to **9**; as a result, an increase of the nitrogen splitting is observed, which is particularly evident for solvents where hydrogen bonding is possible (see structure **11**, Block 8.1).

The stability of nitroxides may be attributed to three factors: electron delocalization within the molecule, steric shielding of the paramagnetic center and stability towards disproportionation. If H–atoms in α-position to the NO moiety are available, disproportionation reactions will be favored, leading to diamagnetic substances. Thus, the majority of stable nitroxides are secondary amine N–oxides without α–hydrogen atoms. Bulky substituents on the α–carbon atoms do not only prevent disproportionation but also the tendency towards dimerization, particularly in the solid state. Thus steric hindrance is mainly responsible for kinetic stability. The more pronounced effect for stability is the electronic configuration of the N-O group. General structures for stable nitroxides are shown in Figure 2.9 with the simplest representative di-*tert*-butylnitroxide DTBN (a). The most common derivates stem from six-membered piperidine rings (b) and five-membered pyrrolidine (c), oxazolidine (d) pyrroline (e) rings. Since chemical structures of nitroxides are relatively complex, trivial names formed by abbreviations are usually employed.

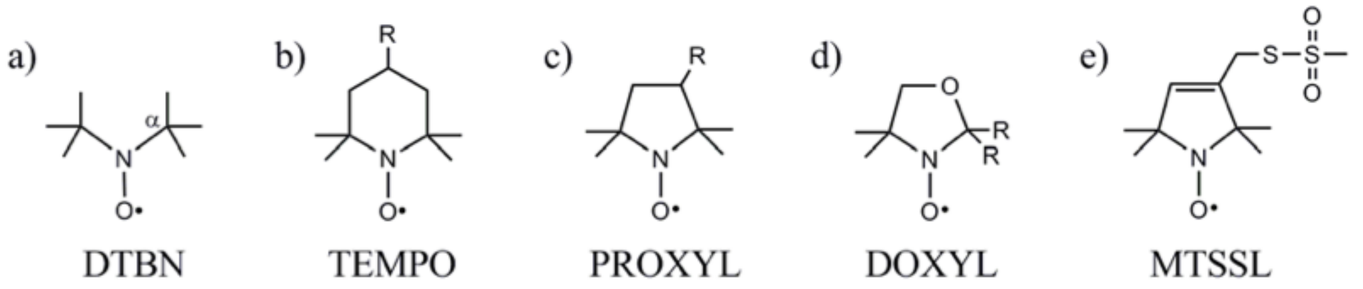

Figure 2.9 The main types of stable nitroxides contain no hydrogen atom at the α-carbon and are cyclic analogs of a) di-*tert*-butyl nitroxide, derivates of b) piperidine, c) pyrrolidine d) oxazolidine and e) pyrroline. Labeling reaction is possible with suitable functional group R. DTBN: di-*tert*-butyl nitroxide, TEMPO: 2,2,6,6-tetramethylpiperidine-*N*-oxyl, PROXYL: 2,2,4,4-tetramethylpyrrolidine-*N*-oxyl, DOXYL: 4,4-dimethyloxazolidine-*N*-oxyl, MTSSL: (*N*-oxyl-2,2,5,5 tetramethylpyrroline-3-methyl)methane thiolsulfonate.

Continuous wave ESR (cw-ESR)

Derivative spectrum

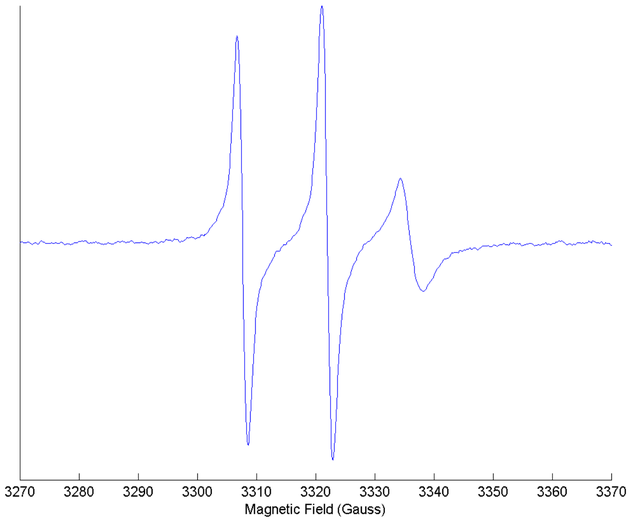

Absorption spectrum

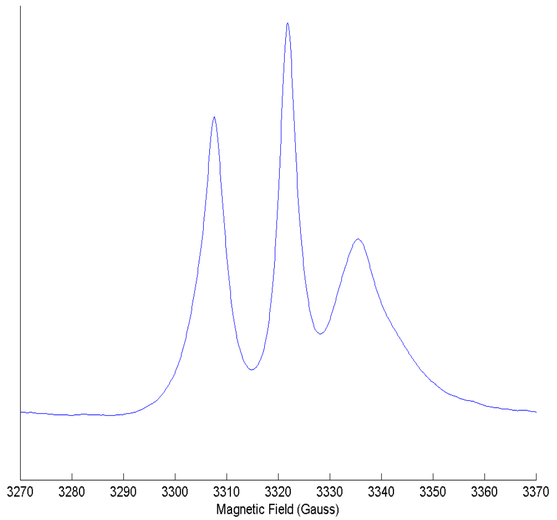

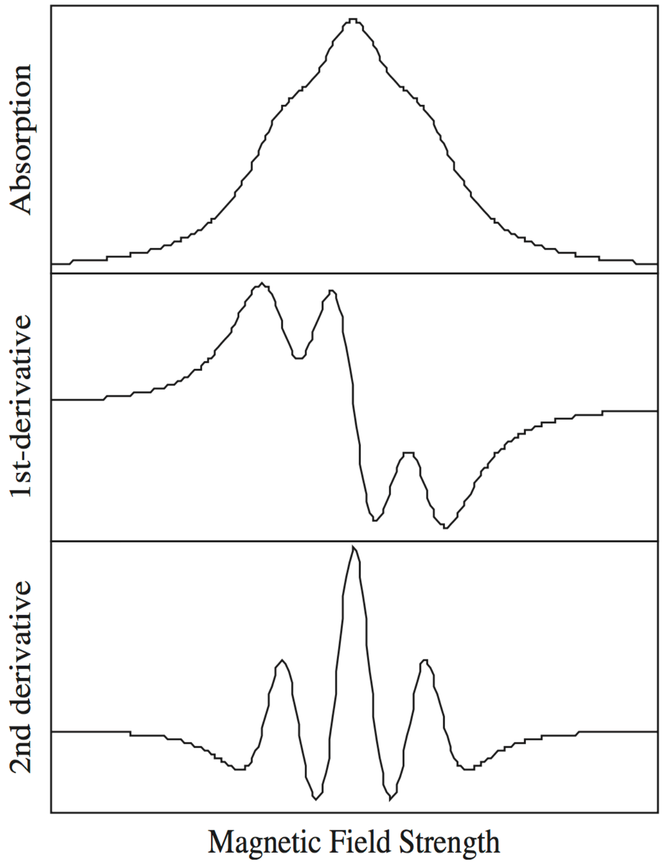

The g-factor: $\Delta E = h\upsilon = g\beta H$

The field at each spin influenced by local magnetic fields, not just the external field :

$$H_{eff} = H + H_{local} \quad so \quad H_{eff} = (1-s)H = (g/g_e)H$$

– This field is induced by ***H***, external field ***H***

– ***g*** is an effective Zeeman factor, shifted from the electron g_e

– The shift in ***g*** is akin to the chemical shift of NMR

– The local induced field comes from the orbital motion of electrons, spin-orbit coupling mixes *J*, *L* and *S* and shifts ***g***, the shift can can be ***g***<2 or ***g***>2. g is thus characteristic of different electronic structures and is also known as the

Landé splitting factor:

$$g = 1 + \frac{J(J+1) + S(S+1) - L(l+1)}{2J(J+1)}$$

- Light atoms, *i.e.*'organic' and first row transition metals with a single unpaired electron can have g close to 2.0
- Heavier atoms, and molecules or atoms with more than one unpaired electron can have g-values very different from 2

A - the hyperfine splitting

- The unpaired electron, which gives us the EPR spectrum, is very sensitive to local fields in its surroundings.
- Local fields arising from magnetic nuclei are *permanent and independent of H. (a · S · I)*
- Interaction with neighboring nuclear magnetic dipoles gives the *nuclear hyperfine interaction* and *hyperfine splitting A*
- Corresponds to the NMR coupling constant J
- For several equivalent nuclei n, $(2n_M I_M + 1)$ transitions are observed for a nucleus M with a spin I
- The relative intensities are given by Pascal's triangle for I = ½

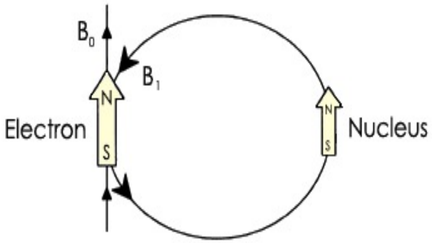

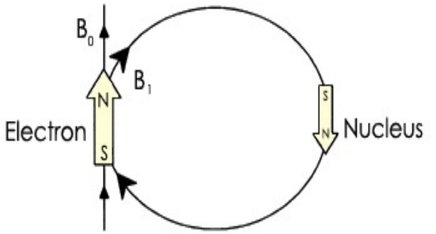

1
1 1
1 2 1
1 3 3 1
1 4 6 4 1
1 5 10 10 5 1

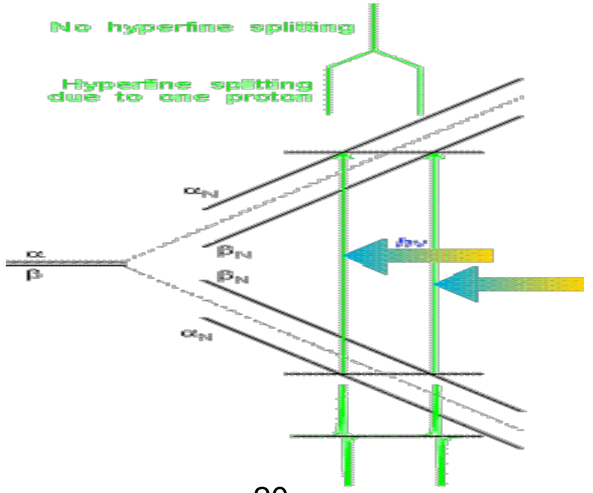

Spin label Electron Spin Resonance

Use spin label to probe the local environment in molecules

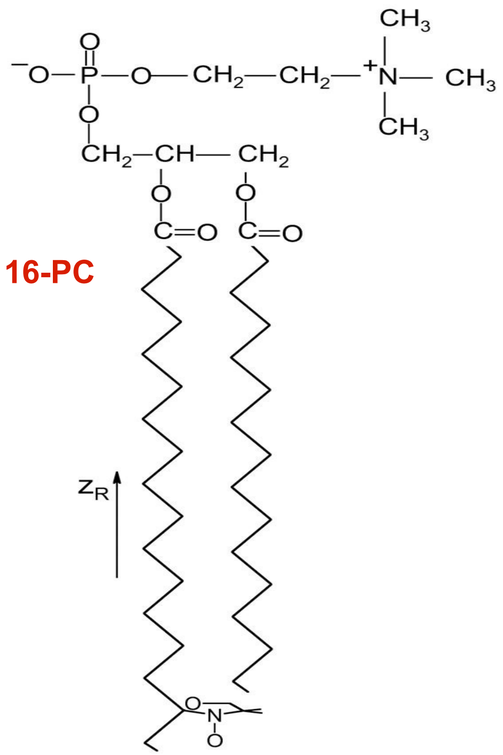

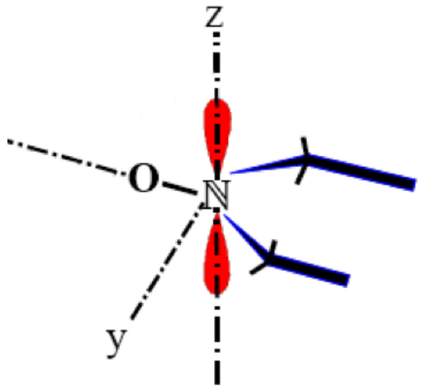

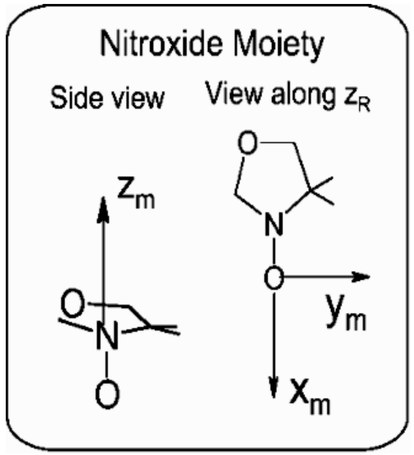

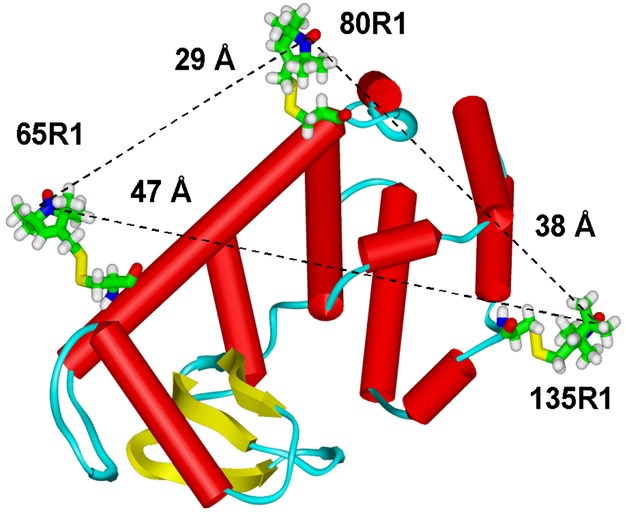

I=1/2 (for ^{15}N)
I=1 (for ^{14}N)

S=1/2

$$Hamiltonian = g\beta HS_z - g_N\beta_N HI_z + a \cdot I \cdot S$$

Electron Zeeman | Nuclear Zeeman | Hyperfine

$$\Delta E = h\nu = g\beta H \qquad \text{(for e-, 1/2-(-1/2)=1)}$$

$$\frac{\Delta E_e}{\Delta E_n} = \frac{g_e\beta_e H}{g_n\beta_n H} \sim 658$$ (more sensitive (per spin) than NMR)

$$\Delta E = h\nu = g\beta H^* \qquad (m_I=0)$$

$$= g\beta H\left(\frac{1}{2} - \left(-\frac{1}{2}\right)\right) + \left(\frac{1}{2}a - \left(-\frac{1}{2}a\right)\right) \qquad (m_I=1)$$

$$= g\beta H + a$$

$$H = H^* - \frac{a}{g\beta} \quad (m_I=1) \qquad \left(for \quad |\alpha_e, m_I = 1\rangle \Leftrightarrow |\beta_e, m_I = 1\rangle\right)$$

$$H = H^* + \frac{a}{g\beta} \quad (m_I=-1) \qquad \left(for \quad |\alpha_e, m_I = -1\rangle \Leftrightarrow |\beta_e, m_I = -1\rangle\right)$$

Overall:

$$H = H^* - \frac{a}{g\beta} m_I$$

in terms of angular freq, ω:
ω=γH for γ=2πgβ/h (gyromagnetic ratio)

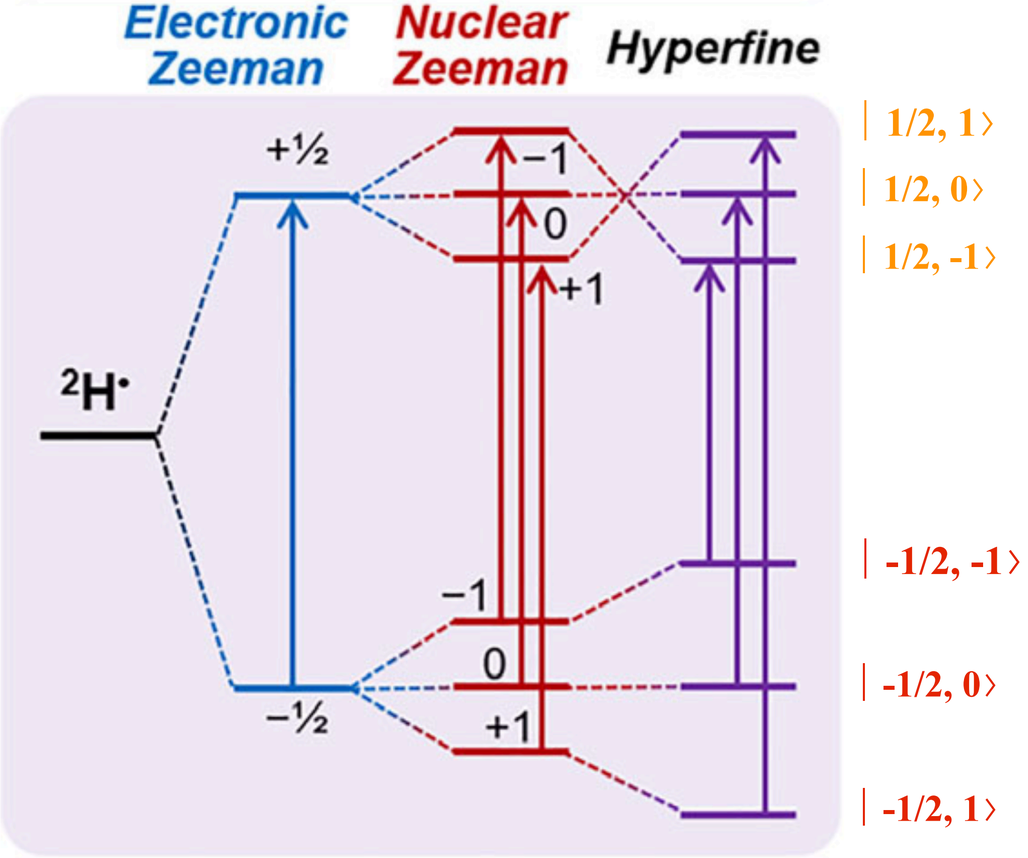

$$H = H^* - m_I A \qquad \text{for} \qquad A = \frac{a}{g\beta}$$

[Gauss]

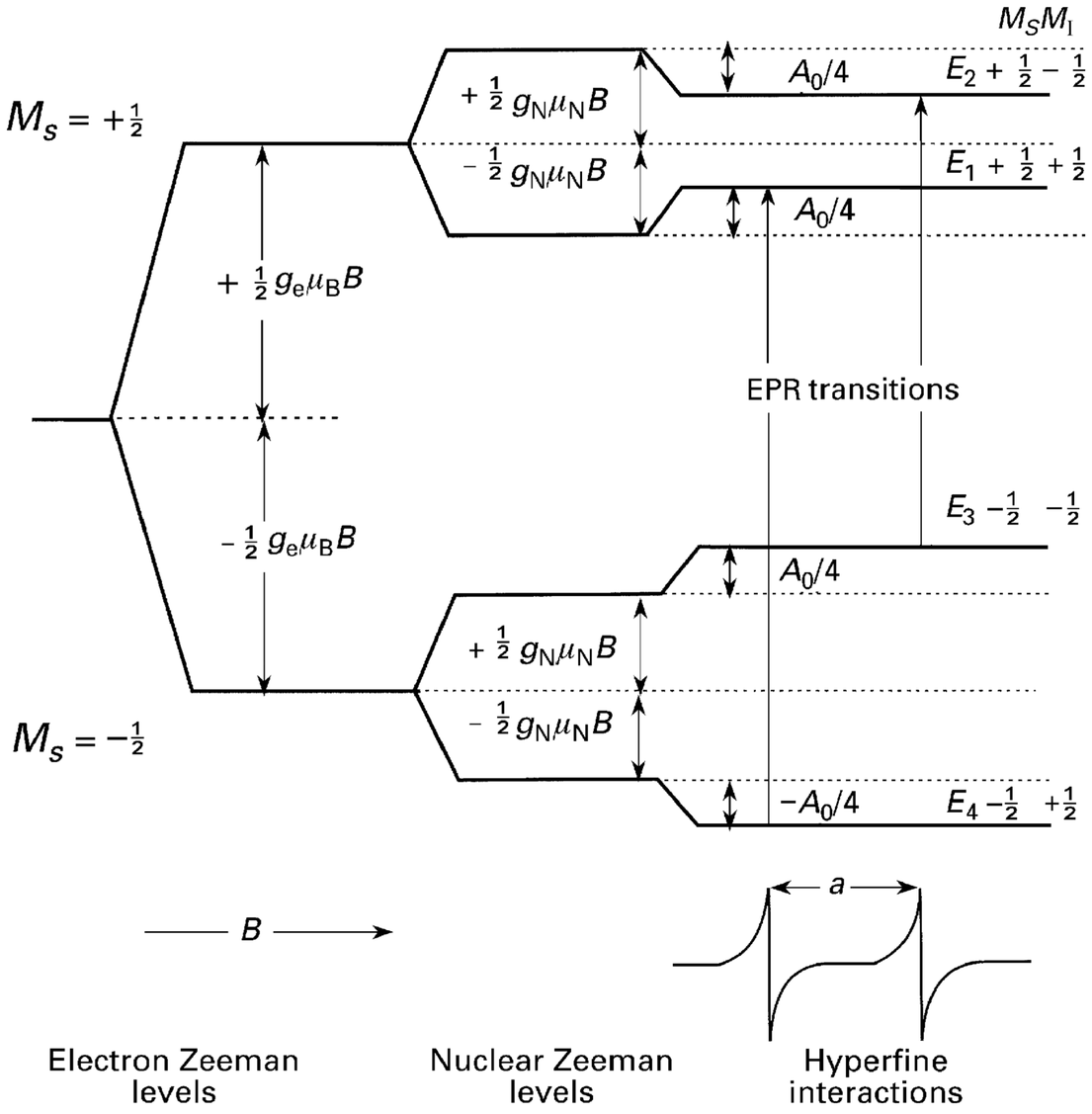

$$E_1 = \tfrac{1}{2} g_e \mu_B B - \tfrac{1}{2} g_N \mu_B B + \tfrac{1}{4} h A_0 \qquad M_S = +\tfrac{1}{2},\ M_I = +\tfrac{1}{2}$$

$$E_2 = \tfrac{1}{2} g_e \mu_B B + \tfrac{1}{2} g_N \mu_N B - \tfrac{1}{4} h A_0 \qquad +\tfrac{1}{2}\ -\tfrac{1}{2}$$

$$E_3 = -\tfrac{1}{2} g_e \mu_B B + \tfrac{1}{2} g_N \mu_N B + \tfrac{1}{4} h A_0 \qquad -\tfrac{1}{2}\ -\tfrac{1}{2}$$

$$E_4 = -\tfrac{1}{2} g_e \mu_B B - \tfrac{1}{2} g_N \mu_N B - \tfrac{1}{4} h A_0 \qquad -\tfrac{1}{2}\ +\tfrac{1}{2}$$

$$\Delta M_I = 0 \quad \text{and} \quad \Delta M_S = \pm 1$$

Thus two resonance transitions can occur at

$$\Delta E_A = E_1 - E_4 = g_e \mu_B B + \tfrac{1}{2} h A_0$$

$$\Delta E_B = E_2 - E_3 = g_e \mu_B B - \tfrac{1}{2} h A_0$$

$$B_1 = \frac{h\nu}{g_e \mu_B} - \frac{h A_0}{2 g_e \mu_B} = \frac{h\nu}{g_e \mu_B} - \frac{a}{2}$$

$$B_2 = \frac{h\nu}{g_e \mu_B} + \frac{h A_0}{2 g_e \mu_B} = \frac{h\nu}{g_e \mu_B} + \frac{a}{2}$$

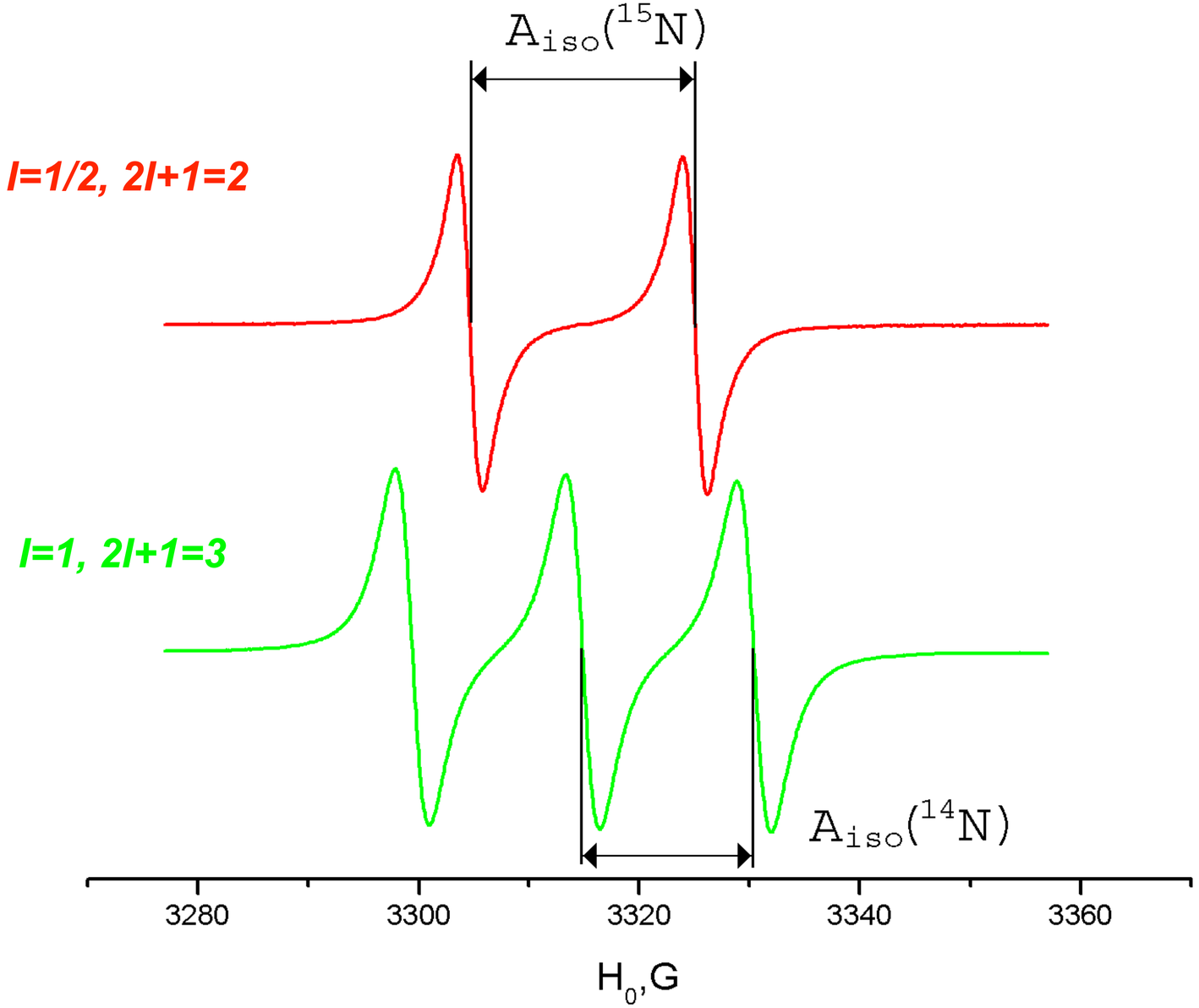
$A_{iso}(^{15}N)$
I=1/2, 2I+1=2
I=1, 2I+1=3
$A_{iso}(^{14}N)$
3280
3300
3320
3340
3360
H_0,G

Anisotropy in g and A

Many measurements are made in the solid state in EPR spectroscopy.

The ability of EPR to obtain useful information from amorphous (glassy) and polycrystalline (powders) as well as from single crystal materials has attracted much biology and biochemistry research

Usually : g_X, g_Y, g_Z are not all equal, so g is anisotropic. Same for A_X, A_Y, A_Z.

For EPR the local symmetry at an unpaired electron center is categorised as :

•*Cubic*. If x = y = z is cubic (*cubal, octahedral, tetrahedral*) No anisotropy in g and A.

•*Uniaxial (Axial)*. If x = y, and z is unique.
Linear rotation symmetry (at least 3-fold). Two principal values each for g and A. For an arbitrary orientation:

$$g_\theta^2 = g_\perp^2 \sin^2\theta + g_{II}^2 \cos^2\theta$$

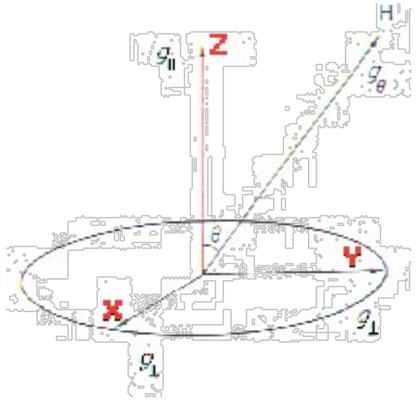

•*Rhombic*. Three unequal components for g and A

For an arbitrary orientation:

$$g^2 = g_{XX}^2 \sin^2\theta\cos^2\phi + g_{YY}^2 \sin^2\theta\sin^2\phi + g_{ZZ}^2 \cos^2\phi$$

⑥ Principle Axes

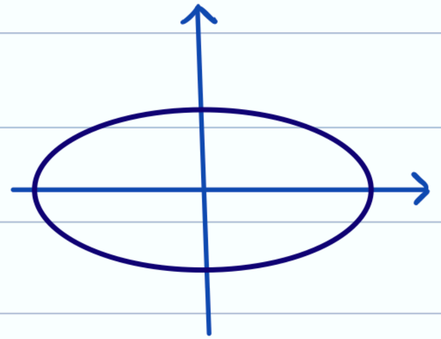

$$\rightarrow \quad x^2 + 4y^2 = 1 = (x, y)\begin{pmatrix} 1 & 0 \\ 0 & 4 \end{pmatrix}\begin{pmatrix} x \\ y \end{pmatrix}$$

$\langle r|$ — B — $|r\rangle$

$$= \langle r \mid B \mid r \rangle$$

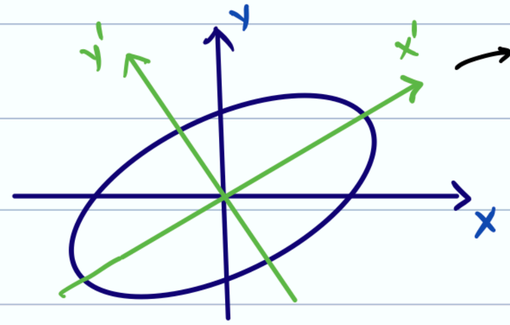

$$\rightarrow \quad \frac{5}{2}x^2 - 3xy + \frac{5}{2}y^2 = 1 = \langle r| \begin{pmatrix} 5/2 & -3/2 \\ -3/2 & 5/2 \end{pmatrix} |r\rangle$$

A

→ To Find principle axes

$$\langle r|A|r\rangle = \langle r|R\,\tilde{R}^{-1}AR\,\tilde{R}^{-1}|r\rangle = \langle r'|\begin{pmatrix} 1 & 0 \\ 0 & 4 \end{pmatrix}|r'\rangle$$

$\langle r'|$ — diag — $|r'\rangle$

$$= \langle r' \mid B \mid r' \rangle$$

new coord. $= \begin{pmatrix} x' \\ y' \end{pmatrix}$

Construction of g matrix

$$\hat{\mathcal{H}} = \beta_e [B_X \quad B_Y \quad B_Z] \cdot \begin{bmatrix} g_\perp & 0 & 0 \\ 0 & g_\perp & 0 \\ 0 & 0 & g_\parallel \end{bmatrix} \cdot \begin{bmatrix} \hat{S}_X \\ \hat{S}_Y \\ \hat{S}_Z \end{bmatrix}$$

magnetic moment

$$\hat{\boldsymbol{\mu}} = \beta_e \mathbf{g} \cdot \hat{\mathbf{S}} \qquad = \beta_e \mathbf{B}^{\mathrm{T}} \cdot g \cdot \hat{\mathbf{S}}$$

which is taken to interact with the field $\mathbf{B}$ (see Eqs. 1.14).

Alternatively, the product $\mathbf{B}^{\mathrm{T}} \cdot \mathbf{g}$ in Eq. 4.4*c* may be regarded as a vector resulting from a transformation of the actual field $\mathbf{B}$ to an effective field

$$\mathbf{B}_{\mathrm{eff}} = \mathbf{g}^{\mathrm{T}} \cdot \mathbf{B}/g_e \tag{4.9a}$$

or equivalently

$$\mathbf{B}_{\mathrm{eff}}{}^{\mathrm{T}} \equiv \mathbf{B}^{\mathrm{T}} \cdot \mathbf{g}/g_e \tag{4.9b}$$

The magnitude of the effective field is given by

$$B_{\mathrm{eff}} = [(\mathbf{g}^{\mathrm{T}} \cdot \mathbf{B})^{\mathrm{T}} \cdot (\mathbf{g}^{\mathrm{T}} \cdot \mathbf{B})]^{1/2}/g_e \tag{4.10a}$$

$$= [\mathbf{B}^{\mathrm{T}} \cdot \mathbf{g} \cdot \mathbf{g}^{\mathrm{T}} \cdot \mathbf{B})]^{1/2}/g_e \tag{4.10b}$$

$$= \{[\mathbf{n}^{\mathrm{T}} \cdot (\mathbf{g} \cdot \mathbf{g}^{\mathrm{T}}) \cdot \mathbf{n})]^{1/2}/g_e\} B \tag{4.10c}$$

$\sqrt{\langle n|g\rangle\langle g|n\rangle}$

$$\mathbf{n} = \mathbf{B}/B = \begin{bmatrix} c_x \\ c_y \\ c_z \end{bmatrix}$$

$$\mathbf{n}^{\mathrm{T}} = \begin{bmatrix} \sin\theta\cos\phi & \sin\theta\sin\phi & \cos\theta \end{bmatrix}$$

is the unit vector along **B**. In concert with Eq. 1.22*b*, we define

$$g = [\mathbf{n}^{\mathrm{T}} \cdot (\mathbf{g} \cdot \mathbf{g}^{\mathrm{T}}) \cdot \mathbf{n})]^{1/2} \qquad \mathbf{n}^{\mathrm{T}} = \begin{bmatrix} \sin\theta\cos\phi & \sin\theta\sin\phi & \cos\theta \end{bmatrix}$$

We adopt the definition $\mathbf{gg} \equiv \mathbf{g} \cdot \mathbf{g}^{\mathrm{T}}$, and now explore some of the properties of this parameter matrix.[2] Even if **g** is asymmetric, **gg** is always symmetric. Thus we need write explicitly only the diagonal and upper off-diagonal elements. In any arbitrary cartesian coordinate system *x*, *y*, *z* fixed in the crystal, **gg** is not diagonal, so that

$$g^2 = \begin{bmatrix} c_x & c_y & c_z \end{bmatrix} \cdot \begin{bmatrix} (\mathbf{gg})_{xx} & (\mathbf{gg})_{xy} & (\mathbf{gg})_{xz} \\ & (\mathbf{gg})_{yy} & (\mathbf{gg})_{yz} \\ & & (\mathbf{gg})_{zz} \end{bmatrix} \cdot \begin{bmatrix} c_x \\ c_y \\ c_z \end{bmatrix} \tag{4.15}$$

Following the procedure outlined in Section A.5.2, we now turn to the general case of the calculation of matrix **gg** from sets of measurements, for which

$$\begin{aligned} g^2 = {} & (\mathbf{gg})_{xx}\sin^2\theta\cos^2\phi + 2(\mathbf{gg})_{xy}\sin^2\theta\cos\phi\sin\phi \\ & + (\mathbf{gg})_{yy}\sin^2\theta\sin^2\phi + 2(\mathbf{gg})_{xz}\cos\theta\sin\theta\cos\phi \\ & + 2(\mathbf{gg})_{yz}\cos\theta\sin\theta\sin\phi + (\mathbf{gg})_{zz}\cos^2\theta \end{aligned} \tag{4.16a}$$

The $(\mathbf{gg})_{ij}$ elements can be determined from experiment by successive rotations of the crystal with $\mathbf{n}$ fixed (or alternatively rotations of the field, i.e., of $\mathbf{n}$, with the crystal fixed) in the xz, yz, and xy planes. For the xz plane ($\phi = 0$), if θ is the angle between $\mathbf{B}$ and the z axis, $c_x = \sin\,\theta$, $c_y = 0$, and $c_z = \cos\,\theta$. Then

$$g^2 = [\sin\theta \quad 0 \quad \cos\theta] \cdot \begin{bmatrix} (\mathbf{gg})_{xx} & (\mathbf{gg})_{xy} & (\mathbf{gg})_{xz} \\ & (\mathbf{gg})_{yy} & (\mathbf{gg})_{yz} \\ & & (\mathbf{gg})_{zz} \end{bmatrix} \cdot \begin{bmatrix} \sin\theta \\ 0 \\ \cos\theta \end{bmatrix} \tag{4.16b}$$

and

$$g^2 = (\mathbf{gg})_{xx}\sin^2\theta + 2(\mathbf{gg})_{xz}\sin\theta\cos\theta + (\mathbf{gg})_{zz}\cos^2\theta \tag{4.16c}$$

Similarly, for rotation in the yz plane ($\phi = 90^\circ$), $c_x = 0$, $c_y = \sin\,\theta$, and $c_z = \cos\,\theta$ so that

$$g^2 = (\mathbf{gg})_{yy}\sin^2\theta + 2(\mathbf{gg})_{yz}\sin\theta\cos\theta + (\mathbf{gg})_{zz}\cos^2\theta \tag{4.17}$$

Likewise, for rotation in the xy plane ($\theta = 90^\circ$), $c_x = \cos\,\phi$, $c_y = \sin\,\phi$, and $c_z = 0$ and hence

$$g^2 = (\mathbf{gg})_{xx}\cos^2\phi + 2(\mathbf{gg})_{xy}\sin\phi\cos\phi + (\mathbf{gg})_{yy}\sin^2\phi \tag{4.18}$$

$$\underbrace{\begin{bmatrix} C_{Xx} & C_{Xy} & C_{Xz} \\ C_{Yx} & C_{Yy} & C_{Yz} \\ C_{Zx} & C_{Zy} & C_{Zz} \end{bmatrix}}_{\mathbf{C}} \cdot \underbrace{\begin{bmatrix} (gg)_{xx} & (gg)_{xy} & (gg)_{xz} \\ & (gg)_{yy} & (gg)_{yx} \\ & & (gg)_{zz} \end{bmatrix}}_{\mathbf{gg}} \cdot \underbrace{\begin{bmatrix} C_{Xx} & C_{Yx} & C_{Zx} \\ C_{Xy} & C_{Yy} & C_{Zy} \\ C_{Xz} & C_{Yz} & C_{Zz} \end{bmatrix}}_{\mathbf{C}^{\mathrm{T}}}$$

$$= \underbrace{\begin{bmatrix} (gg)_X & 0 & 0 \\ & (gg)_Y & 0 \\ & & (gg)_Z \end{bmatrix}}_{\mathbf{d_{gg}}} \tag{4.19}$$

Idea: single crystal ==> obtain matrix gg ==> solve for C matrix ==> diagonal matrix obtained.

Rotation matrix

$$R = \begin{pmatrix} \cos\alpha\cos\beta\cos\gamma - \sin\alpha\sin\gamma & \sin\alpha\cos\beta\cos\gamma + \cos\alpha\sin\gamma & -\sin\beta\cos\gamma \\ -\cos\alpha\cos\beta\sin\gamma - \sin\alpha\cos\gamma & -\sin\alpha\cos\beta\sin\gamma + \cos\alpha\cos\gamma & \sin\beta\sin\gamma \\ \cos\alpha\sin\beta & \sin\alpha\sin\beta & \cos\beta \end{pmatrix}$$

When only g is taken into consideration …

g_x=2.0091, g_y=2.0061, g_z=2.0023

The field shift between the X- and Z- orientations is

$\Delta H = h\nu/g_x\beta - h\nu/g_z\beta \cong h\nu\Delta g/4\beta \sim 11G$

$$\Delta E = h\nu = g\beta H$$

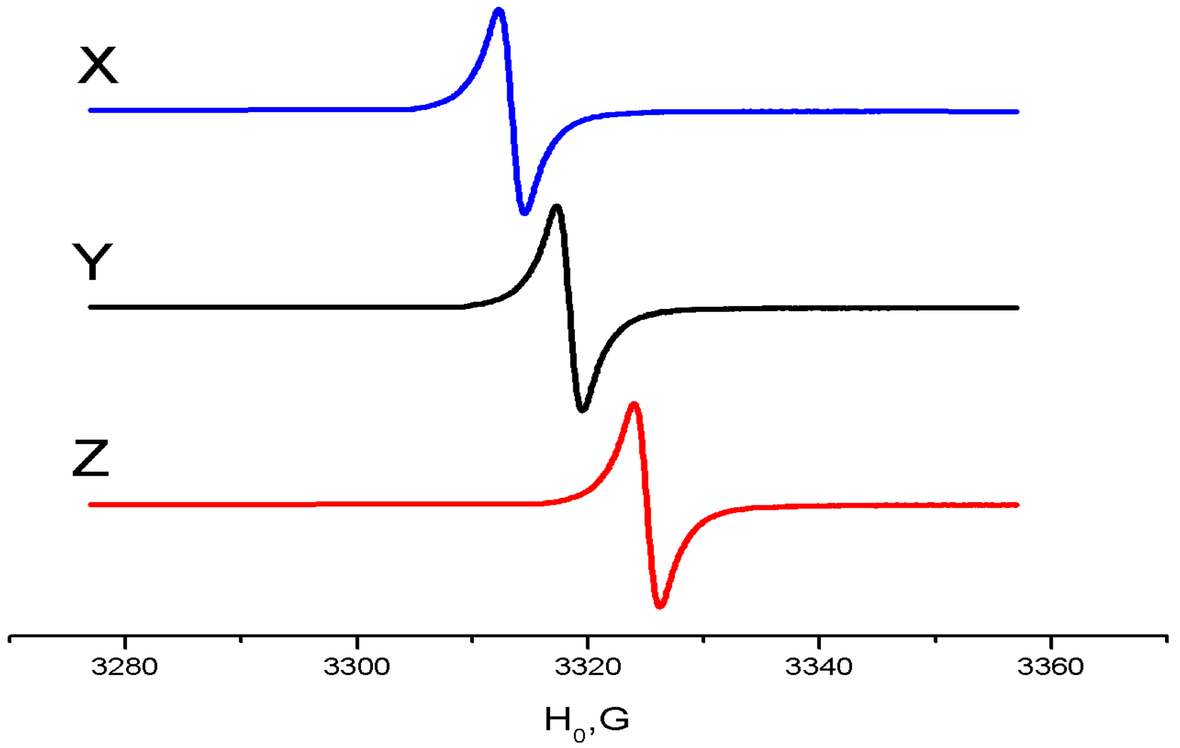

g_x=2.0091, g_y=2.0061, g_z=2.0023

I=1/2, A_x= 6.2, A_y = 6.3, A_z=33.6

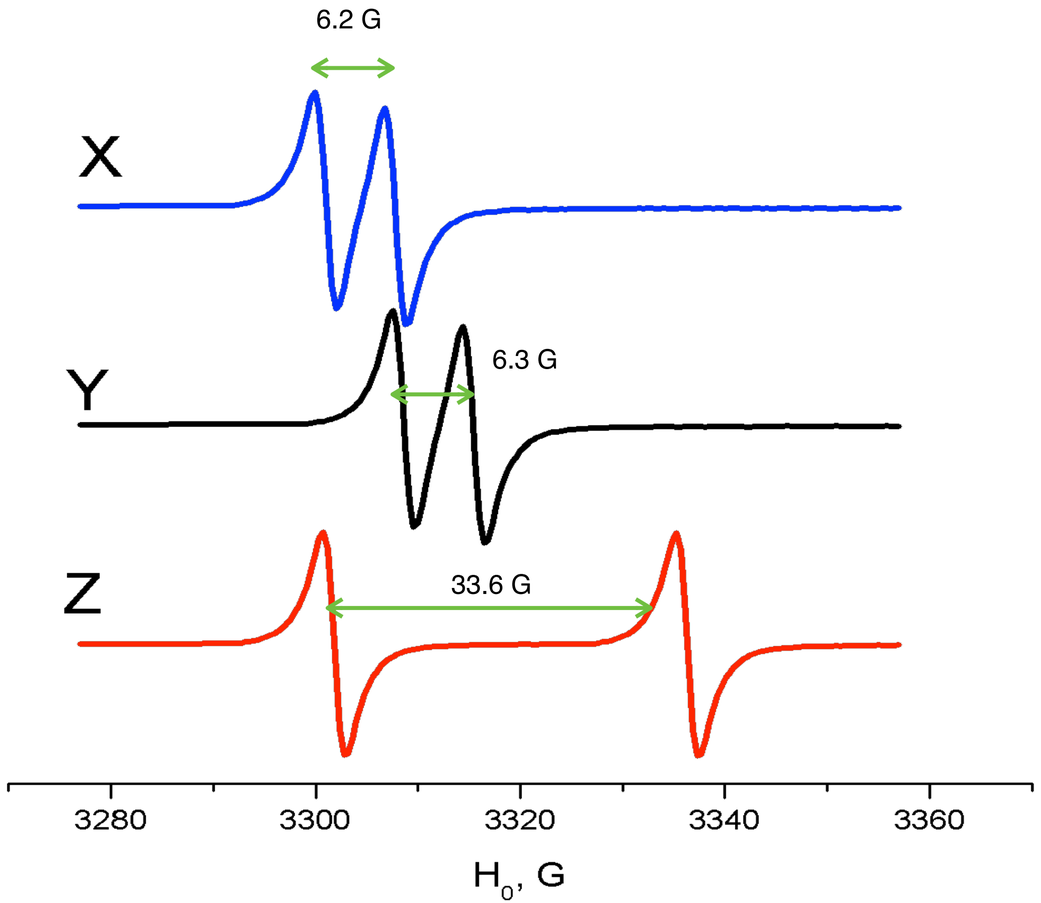

$$H = H^* - \frac{a}{g\beta} m_I$$

$$= \frac{h\nu}{g\beta} - A\, m_I$$

$$= \frac{h\nu}{\beta g(\theta,\phi)} - m_I A(\theta,\phi)$$

g_x=2.0091, g_y=2.0061, g_z=2.0023
I=1, A_x= 6.2, A_y = 6.3, A_z=33.6

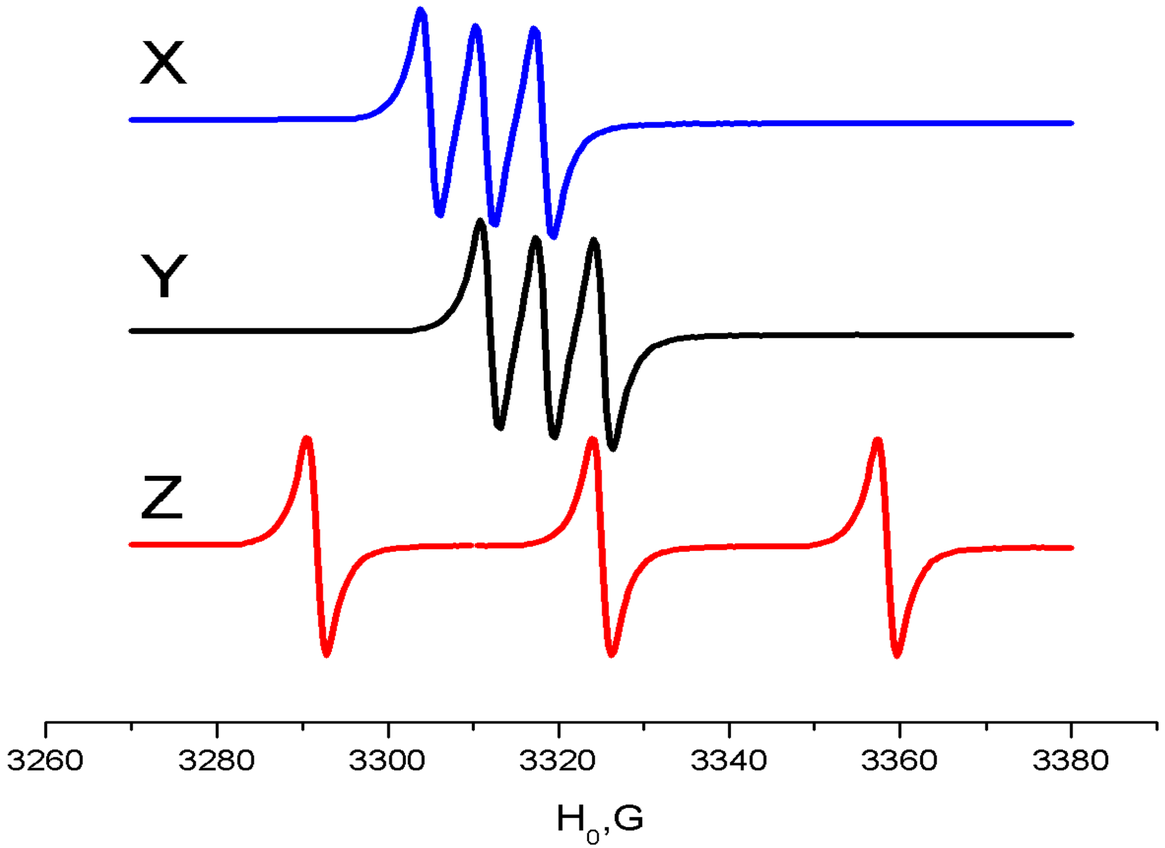

Powder spectra

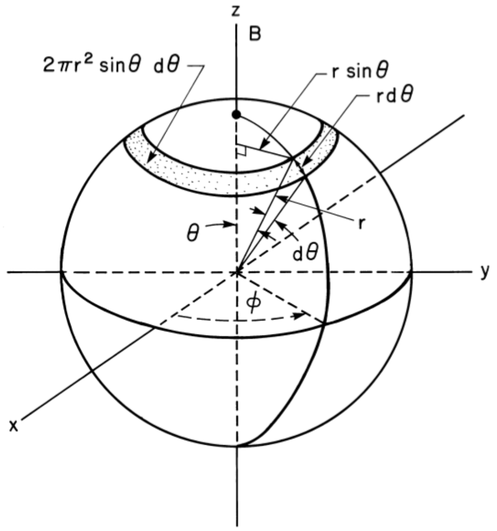

S=1/2, I=0, $g_x=g_y<>g_z$ ***Axially symmetric g-factor***

$$H_r = \frac{h\nu}{g_{eff}\beta} = \frac{h\nu}{\beta}[g_{II}^2\cos^2\theta + g_\perp^2\sin^2\theta]^{-1/2}$$

θ is the angle between a given symmetry axis and the magnetic field direction

The given solid angle Ω is defined to be the ratio of the surface area A to the total surface area on the sphere: $\Omega = A/4\pi r^2$

$d\Omega = 2\pi r^2 \sin\theta d\theta / 4\pi r^2 = \sin\theta d\theta / 2$

$$P(H)dH \propto \sin\theta d\theta \qquad P(H) \propto \frac{\sin\theta}{dH/d\theta}$$

$$P(H) \propto \frac{\beta}{h\nu}\frac{(g_{II}^2\cos^2\theta + g_\perp^2\sin^2\theta)^{3/2}}{(g_{II}^2 - g_\perp^2)\cos\theta}$$

$$P(H) \propto \frac{\beta}{h\nu}\frac{1}{H_r^3(g_{II}^2 - g_\perp^2)\cos\theta}$$

- The probability P(H)dH of a spin system experiencing a resonant field between H and H+ dH

The 'effective field' B_{eff} experienced by the electron spin is a superposition of the internal and external fields and the energy of this anisotropic interaction is given by:

energy= $H_{EZ} = g_e \frac{\mu_B}{\hbar} \boldsymbol{B}_{eff} \boldsymbol{S} = \frac{\mu_B}{\hbar} \boldsymbol{B}_0^T \, \mathbf{g} \, \boldsymbol{S},$

(Note: Hamiltonian = hν = $\hbar\omega$; ω [Energy] = hν / $\hbar$; μ_B=β)

$$= \frac{\mu_B}{\hbar} (B_{0,x} \, B_{0,y} \, B_{0,z}) \begin{pmatrix} g_{xx} & & \\ & g_{yy} & \\ & & g_{zz} \end{pmatrix} \begin{pmatrix} S_x \\ S_y \\ S_z \end{pmatrix}$$

(Note: $U^{-1}AU$=diag; <BIGIS> = <BIU diag(G) U^{-1}IS>
= <B0 I diag(G) I S0>)

Often used definitions

$$g_{\text{iso}} = \frac{1}{3}(g_{xx} + g_{yy} + g_{zz}) = \frac{1}{3} trace(\mathbf{g})$$

$$\Delta g = g_{zz} - g_{iso} \qquad \eta = \frac{g_{yy} - g_{xx}}{\Delta g}$$

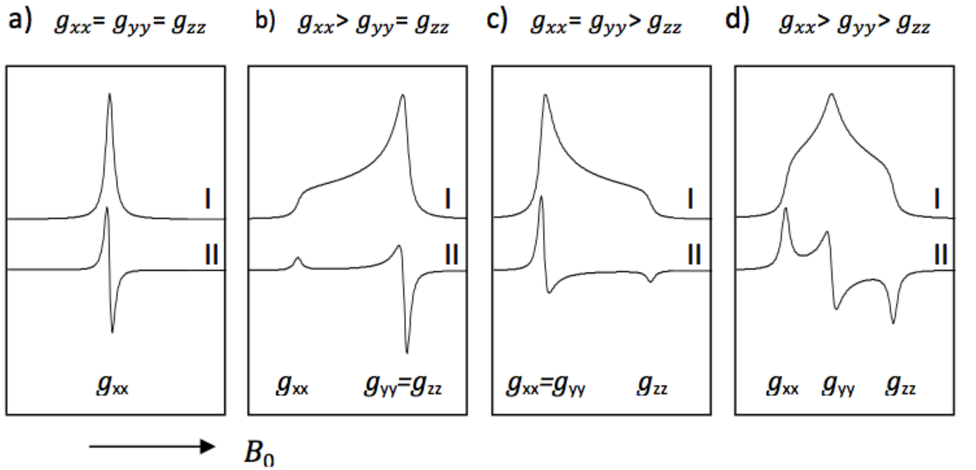

Figure 2.3 Simulated EPR spectra in absorption (I) and first derivative (II) mode for isotropic (a), axial (b,c) and rhombic (d) g-tensor.

On the basis of the element pattern of the **g**-matrix several cases of matrix symmetry can be distinguished, namely isotropic, axial, or rhombic. Examples for powder EPR spectra for different **g**-anisotropies are shown in Figure 2.3.

g_x=2.0091, g_y=2.0061, g_z=2.0023

I=1, A_x= 6.2, A_y = 6.3, A_z=33.6

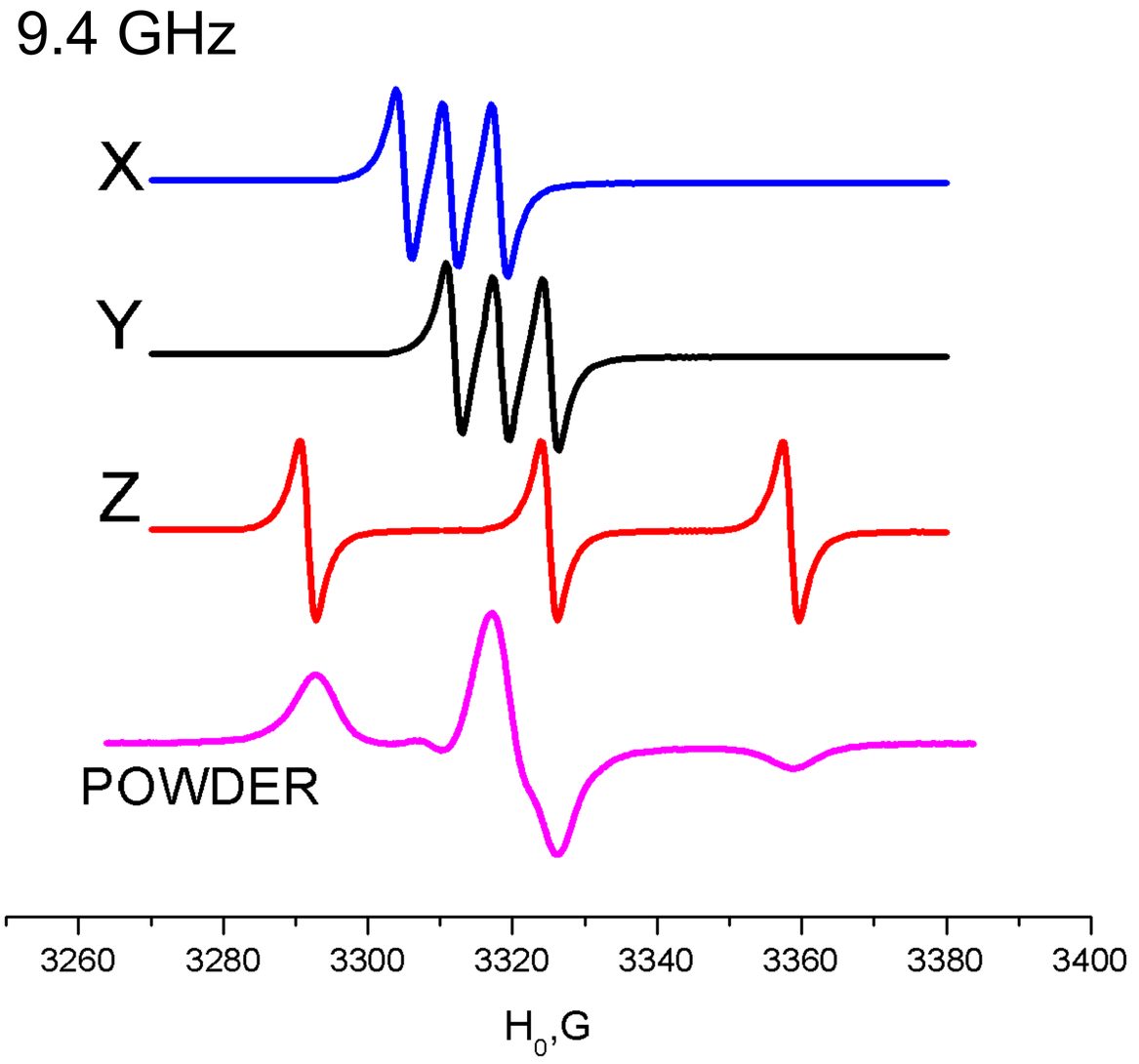

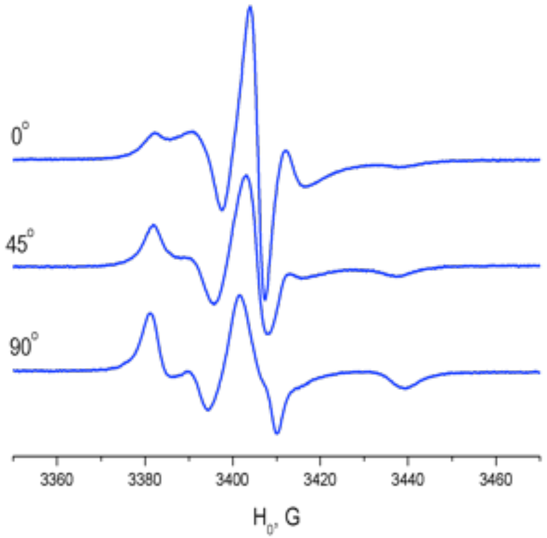

Real data is blurred due to mosaicity

MOMD: microscopic order – macroscopic disorder.
An important case in biology

All orientations of the membrane normal relative to the magnetic field are averaged in vesicles:

g_x=2.0091, g_y=2.0061, g_z=2.0023
I=1, A_x= 6.2, A_y = 6.3, A_z=33.6

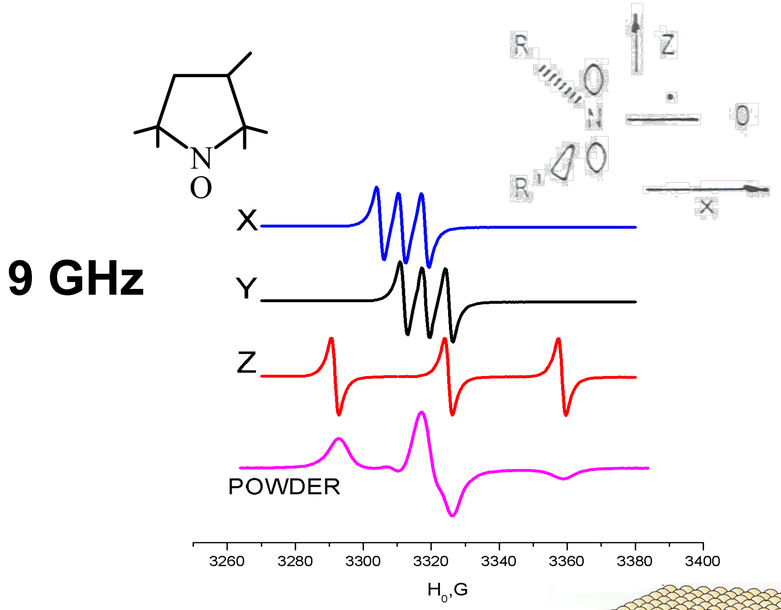

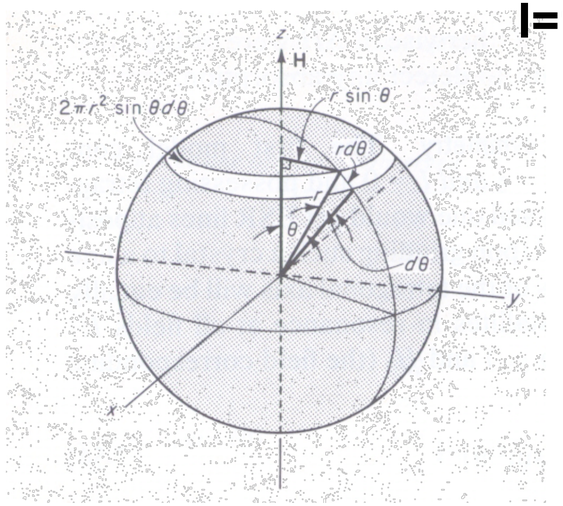

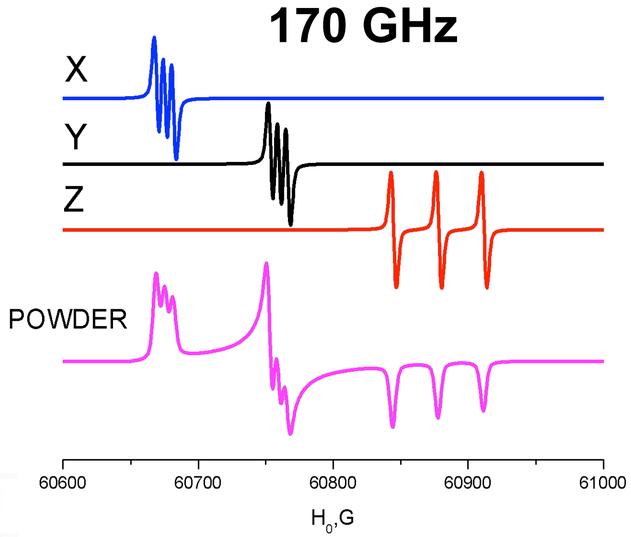

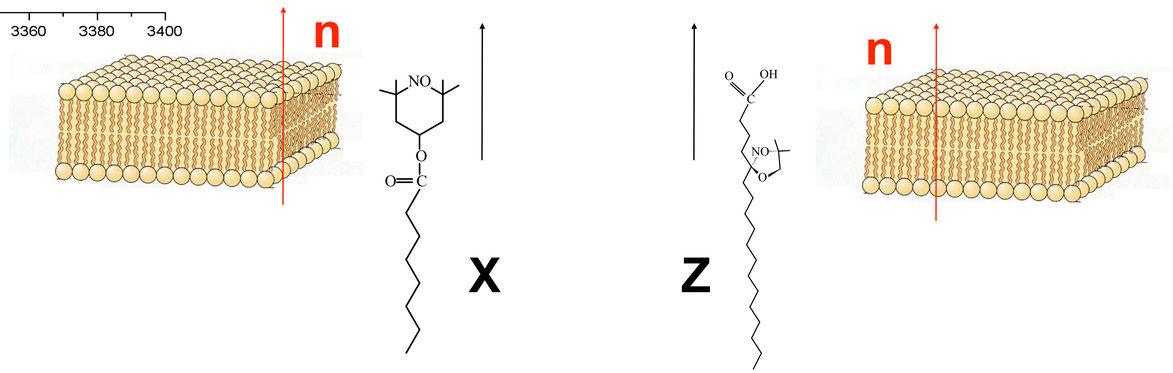

For a macroscopically disordered sample the orientation of the nitroxide moiety manifests itself as a result of anisotropic molecular motion around the principal axis of the molecular frame

Microscopic Ordered and Macroscopic Disorder (MOMD)

e.g. Membrane Vesicles

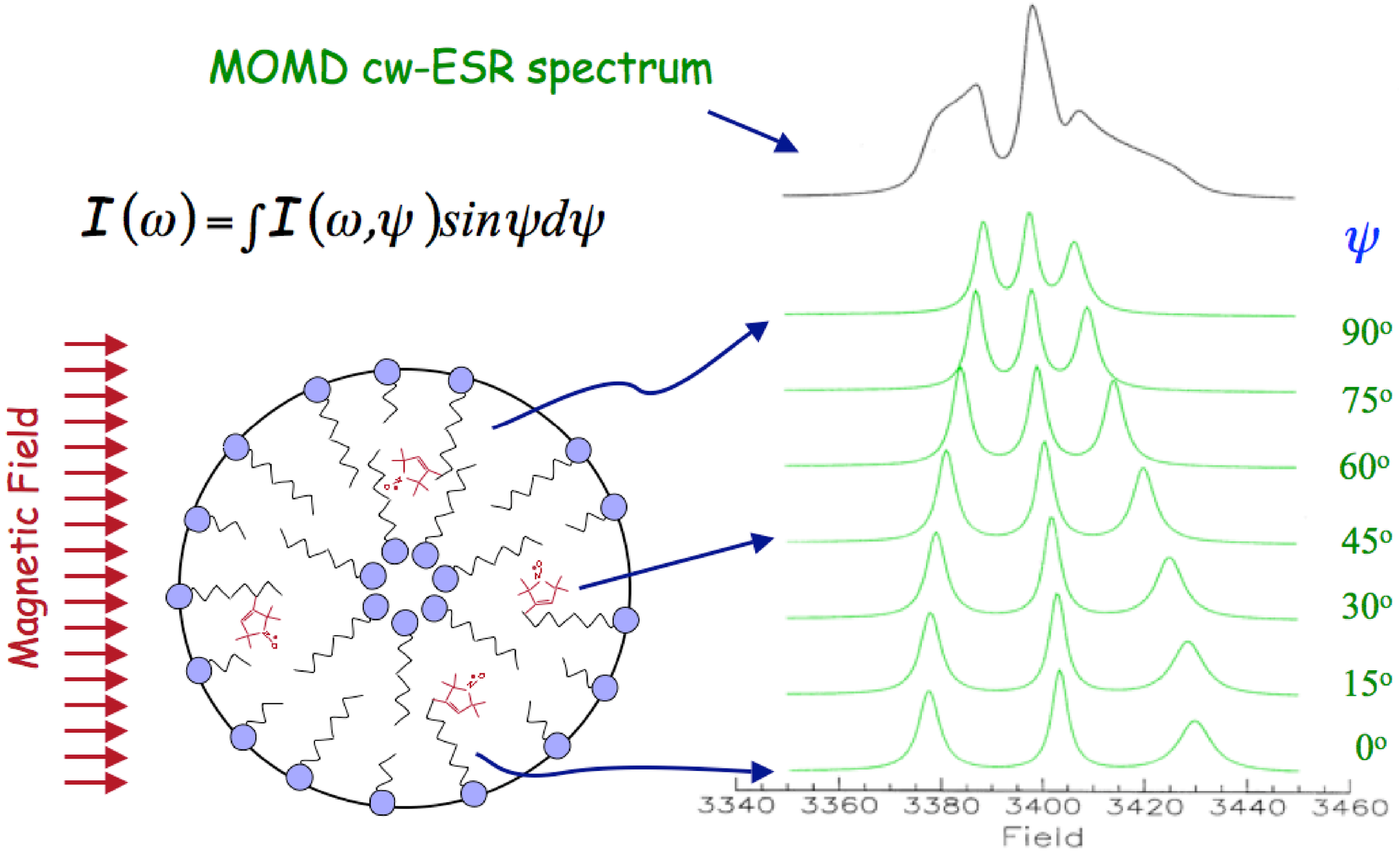

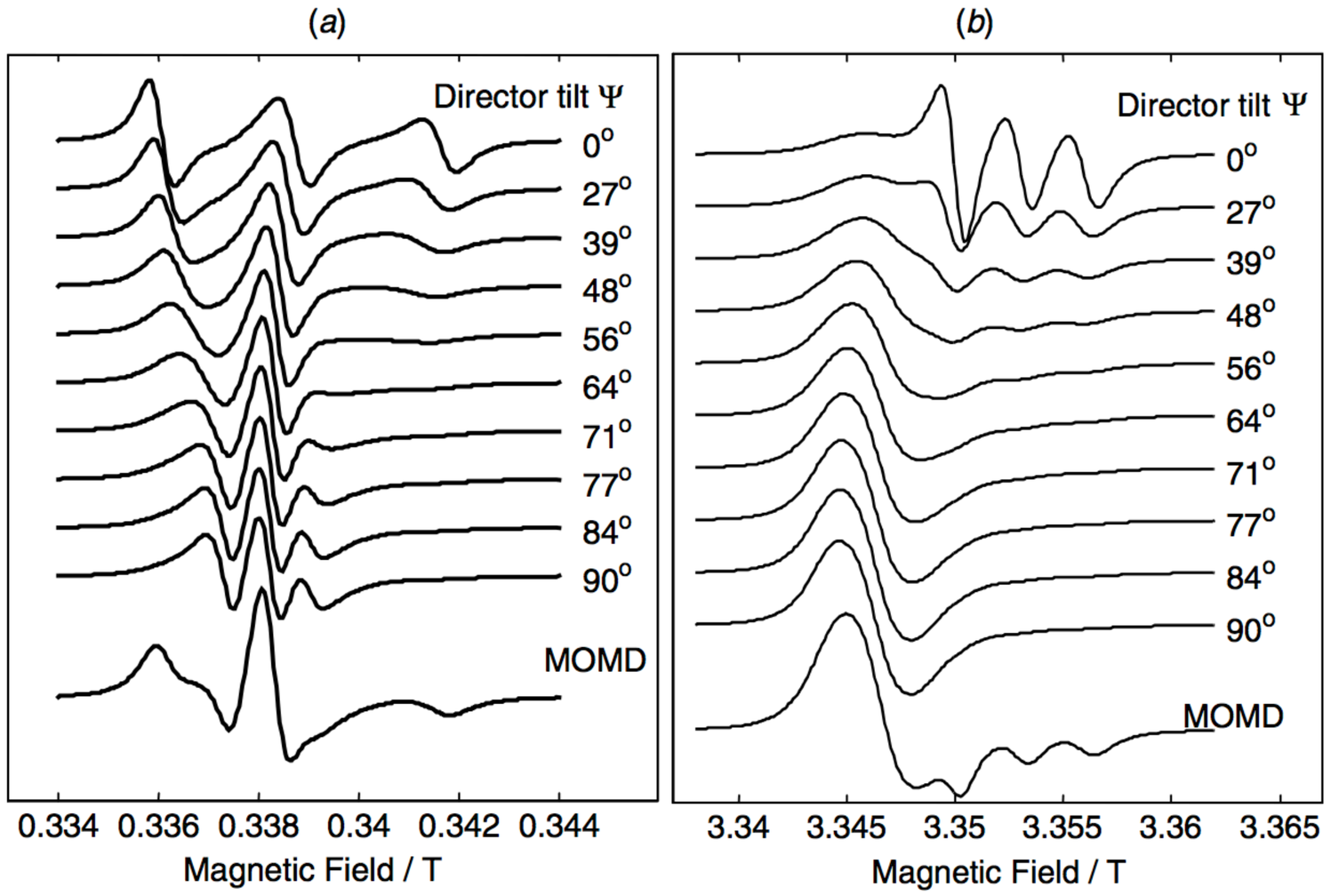

Fig. 12. Components of a MOMD ESR spectrum of a nitroxide spin label, showing the individual spectra from domains with different tilt angles, and integrated MOMD spectrum at the bottom, for 9 GHz (left-hand side) and 94 GHz (right-hand side).

High field EPR spectroscopy is the ***g-resolved spectroscopy***, the regions corresponding different orientations of the magnetic axis relative to the external magnetic field

do not overlap

$$H = H^* - \frac{a}{g\beta} m_I$$

$$= \frac{h\nu}{g\beta} - A\, m_I$$

$$= \frac{h\nu}{\beta g(\theta,\phi)} - m_I A(\theta,\phi)$$

$$H = \frac{h\upsilon}{g\beta}$$

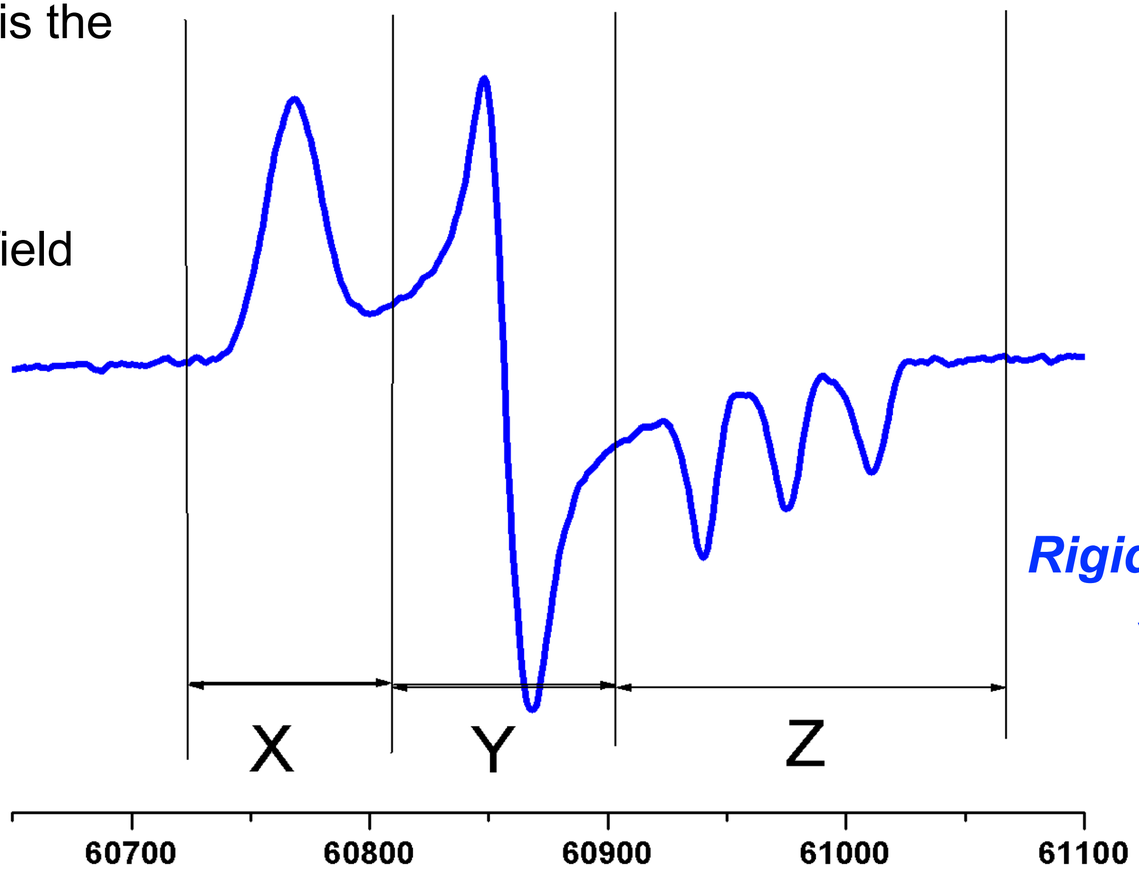

Rigid-limit (frozen) spectrum

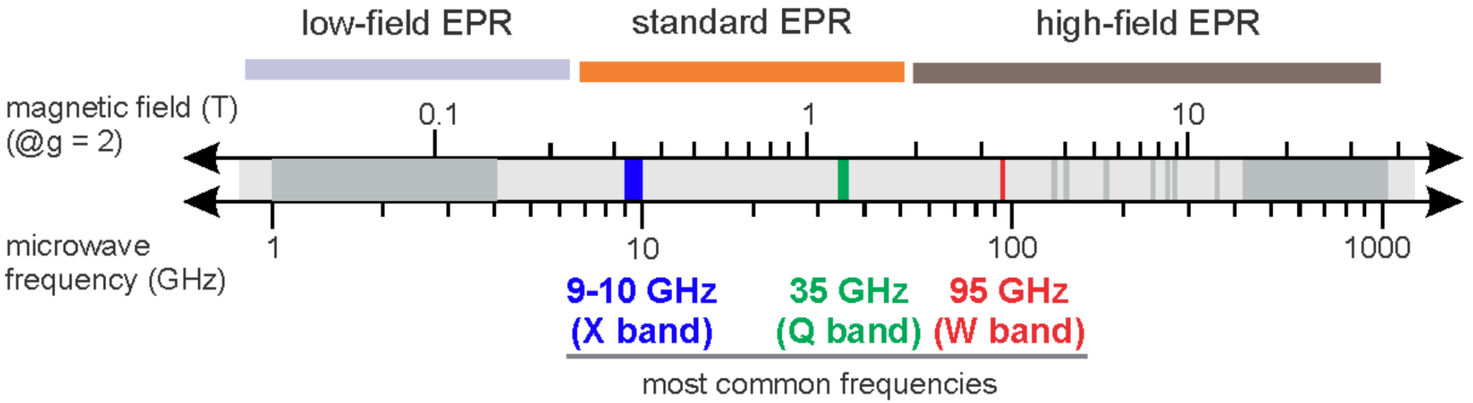

g_x=2.0091, g_y=2.0061, g_z=2.0023

I=1, A_x= 6.2, A_y = 6.3, A_z=33.6

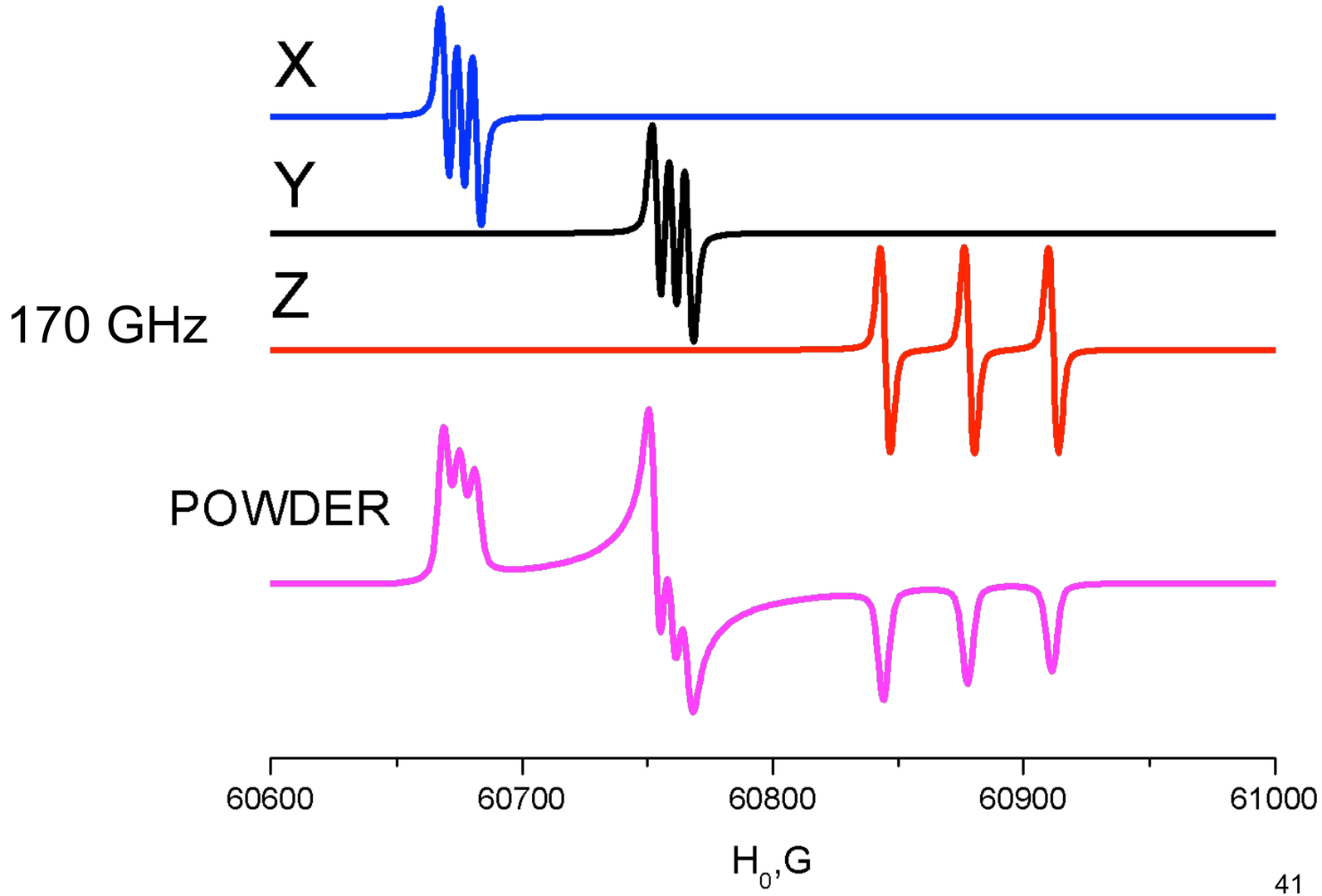

(a) X-band Spectrum

Dominated by HF-term

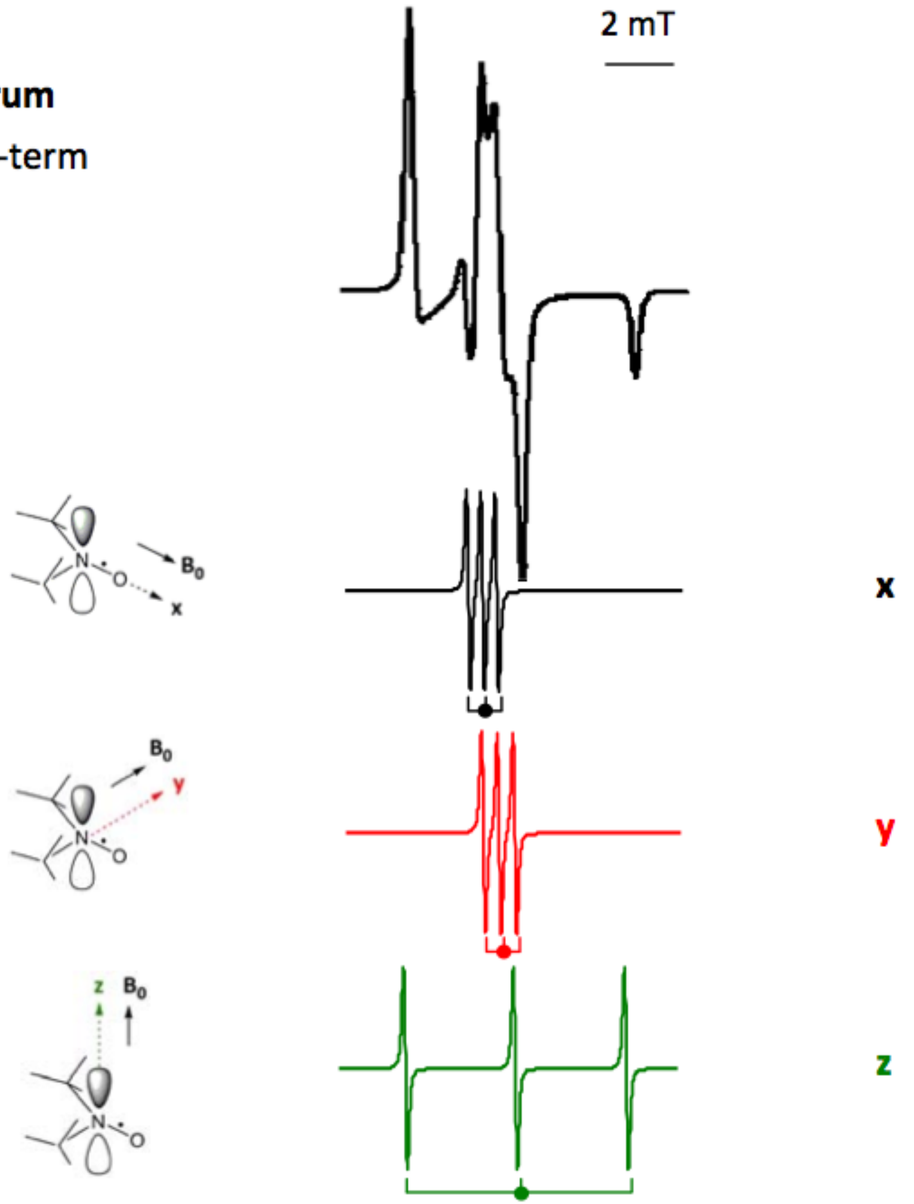

(b) W-band Spectrum

Dominated by EZ-term

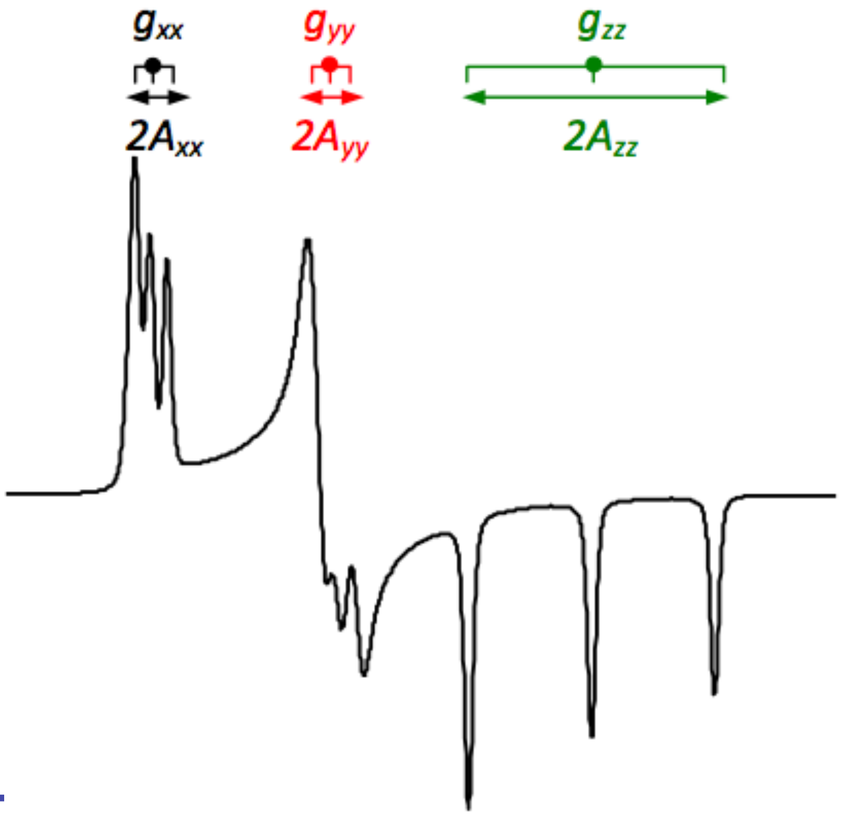

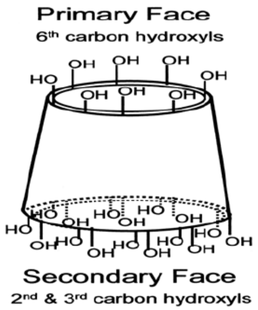

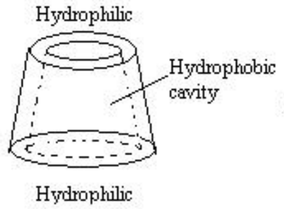

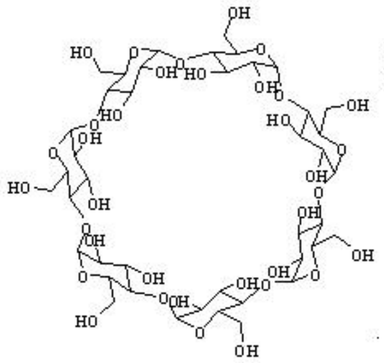

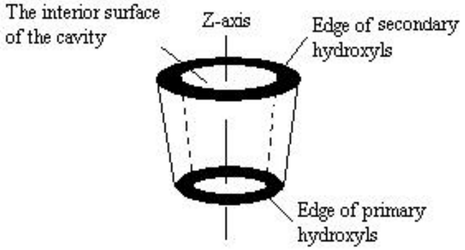

Cyclodextrins (CDs) are cyclic oligomers of D-glucopyranose. Due to the presence of a hydrophobic cavity in the molecule they are able to form guest–host complexes with a variety of organic compounds.

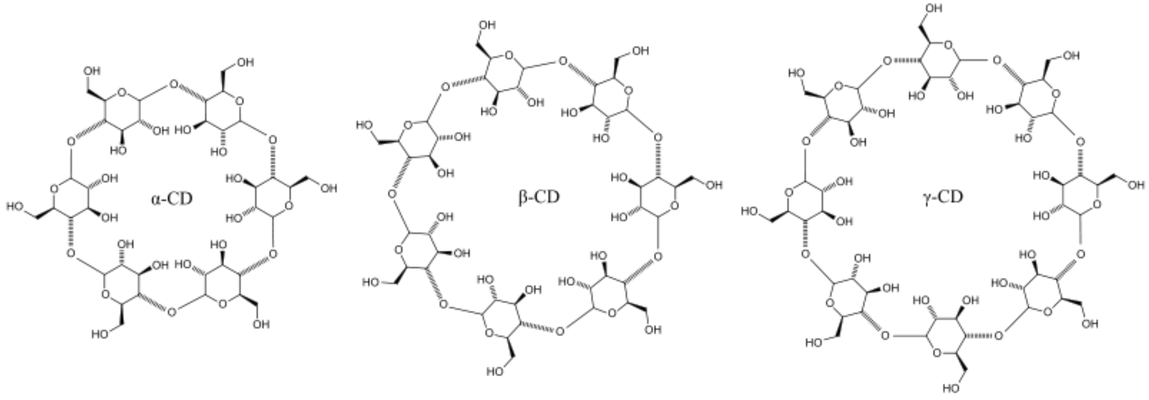

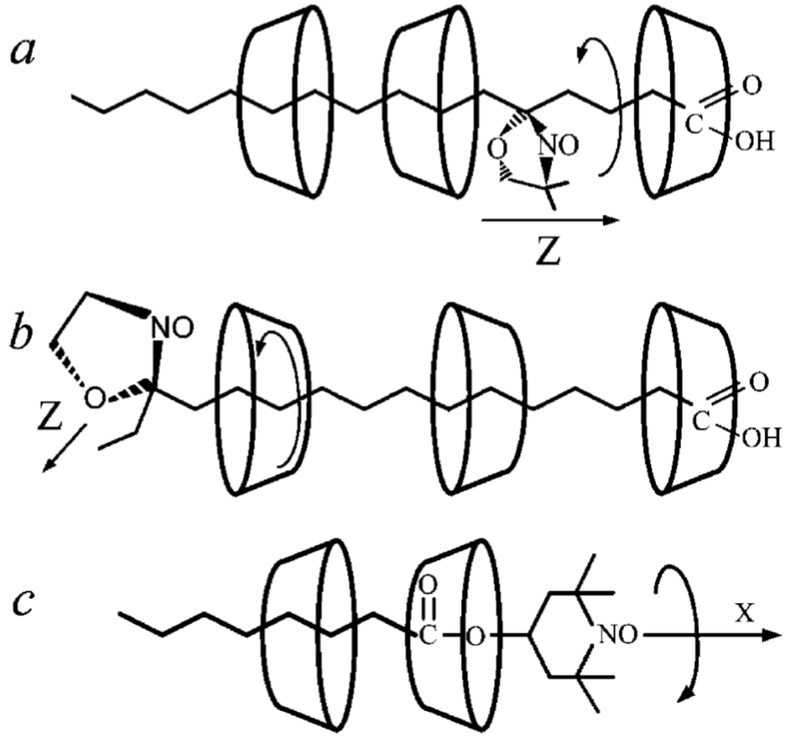

Fig. 7 Schematic drawing of the hypothetical arrangement of cyclodextrin molecules around spin-labeled compound: (a) 5-sasl (b) 16-sasl (c) TEMPOyl-caprylate.

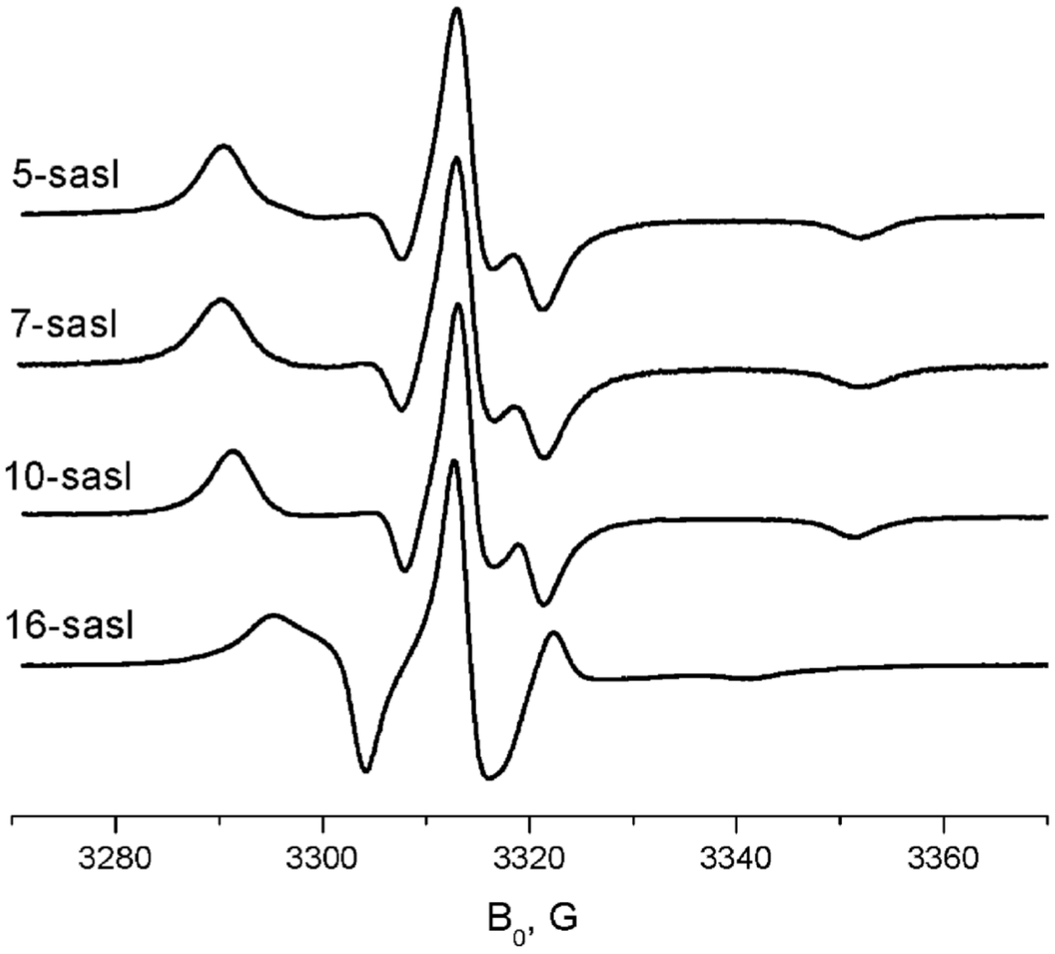

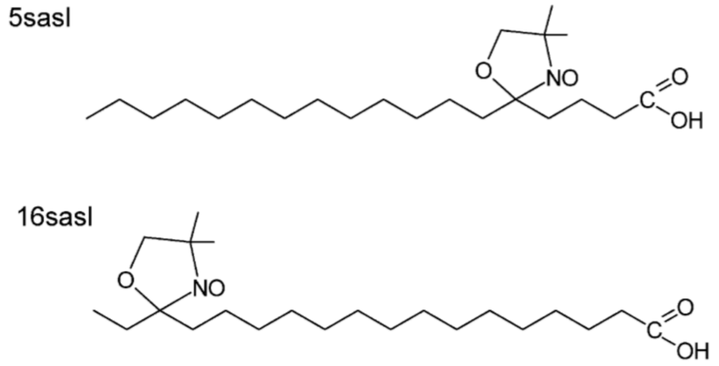

- **Slow-motional spectra, rigid-limit like at room T. (except 16-sasl)**
- **Less lineshape change at 9 GHz ==> less dynamical information.**
- **Sample condition: solid like with some crystallohydrate water.**

Fig. 4 9 GHz spectra of 5-, 7-, 10- and 16-doxyl stearic acids at 293 K in solid γ-CD.

HFHF ESR provides better orientational resolution.

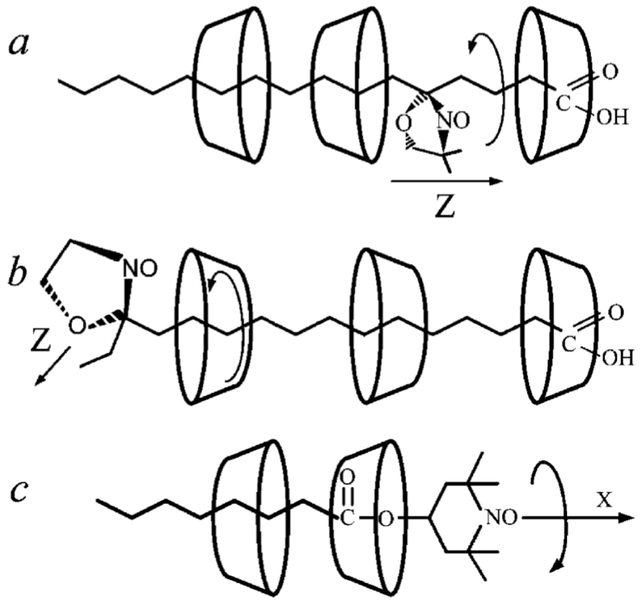

Fig. 7 Schematic drawing of the hypothetical arrangement of cyclodextrin molecules around spin-labeled compound: (a) 5-sasl (b) 16-sasl (c) TEMPOyl-caprylate.

240 GHz, 5-sasl in γ-CD

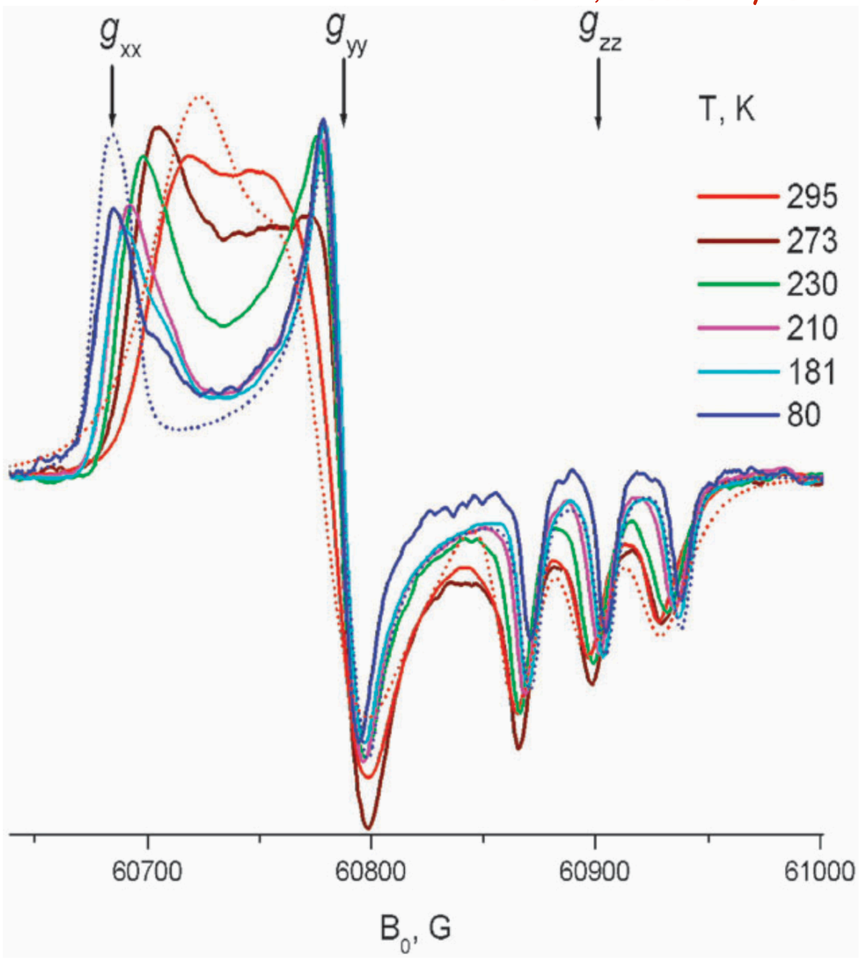

Fig. 5 170 GHz spectra of 5-sasl in solid γ-CD at 80–295 K. Dotted lines show simulations for 80 K (rigid limit) and 295 K.

As a result, once motional effects are discernable in the spectrum, one can discern about which axis (or axes) the motion occurs.

At low T it enables the unambiguous determination of the A and the g tensors.

At high T but in solid state (not tumbling motions), local enhanced rotation improves the spectral resolution; low-field region is blurred by the motion-induced ambiguity effect.

HFHF ESR provides better orientational resolution.

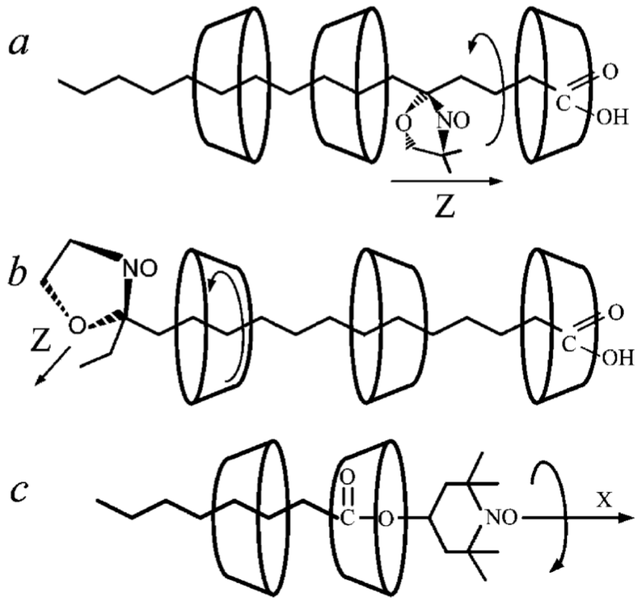

Fig. 7 Schematic drawing of the hypothetical arrangement of cyclodextrin molecules around spin-labeled compound: (a) 5-sasl (b) 16-sasl (c) TEMPOyl-caprylate.

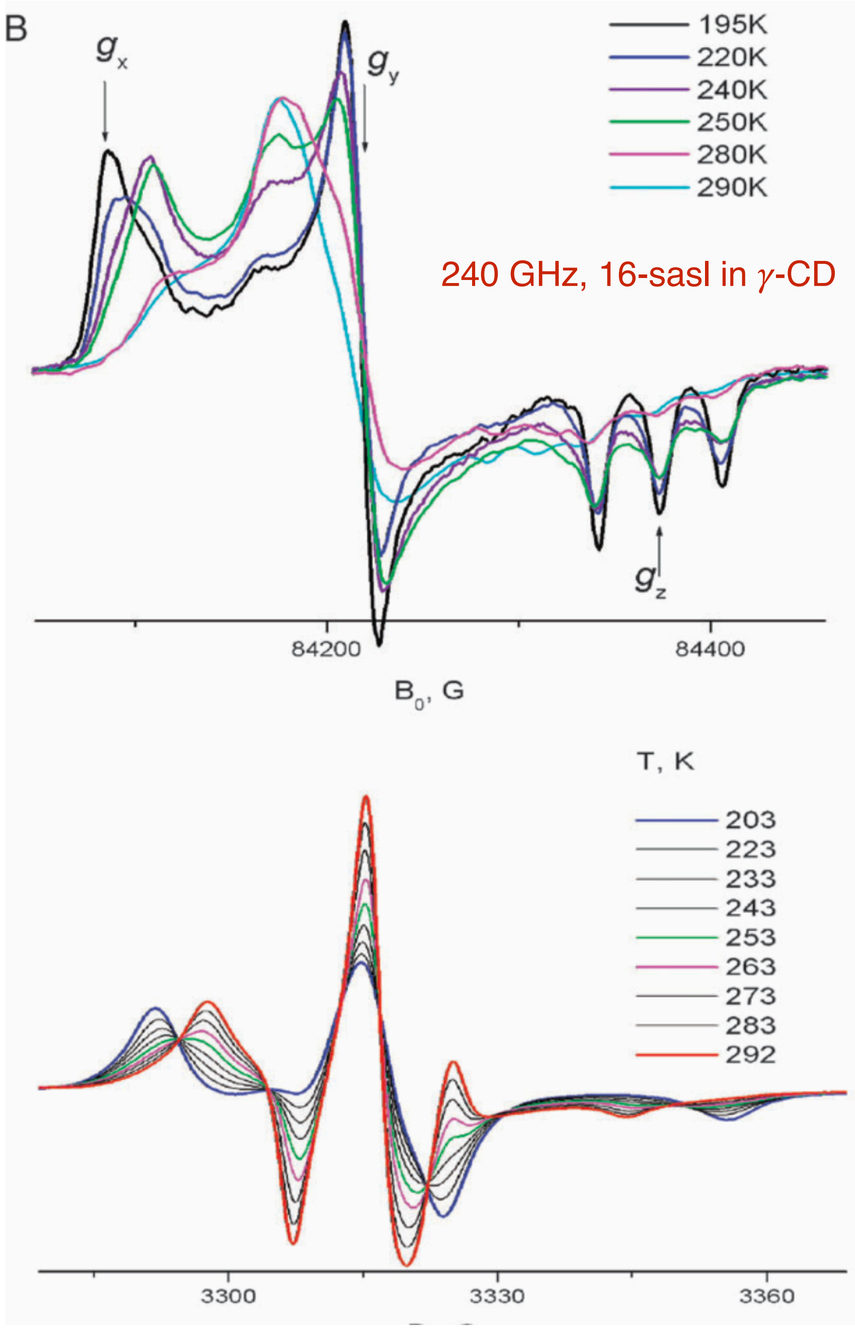

As a result, once motional effects are discernable in the spectrum, one can discern about which axis (or axes) the motion occurs.

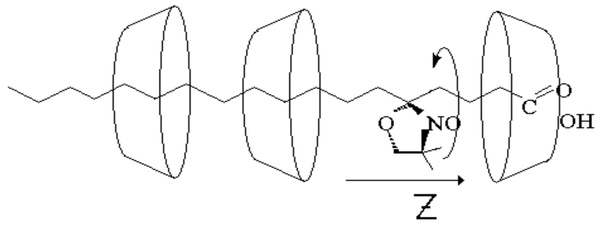

Z-rotation vs. slow motion

5 sasl wet
5 sasl pumped

9.4 GHz

170 GHz

Averaging *effective* tensor components

$(g_{xx}+ g_{yy})/2, (g_{xx}+ g_{yy})/2, g_{zz}$

$(A_{xx}+ A_{yy})/2, (A_{xx}+ A_{yy})/2\ A_{zz}$

Averaging real tensor components

$g_{xx}, g_{yy}, g_{zz}, A_{xx}, A_{yy}, A_{zz}$

3040 3060 3080 3100 3120 3140 3160 3180

Room T

60600 60700 60800 60900 61000 61100 61200

HFHF ESR allowed us to demonstrate Z- and X-axial rotation and determine the relevant rotational diffusion constants and potential barriers. Such determination at 9 GHz is either impossible (Z-rotation) or inaccurate (X-rotation).

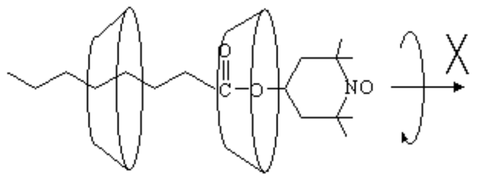

X-rotation

Averaging *effective* tensor components

g_{xx}, $(g_{yy}+ g_{zz})/2$, $(g_{yy}+ g_{zz})/2$,

A_{xx}, $(A_{yy}+ A_{zz})/2$, $(A_{yy}+ A_{zz})/2$

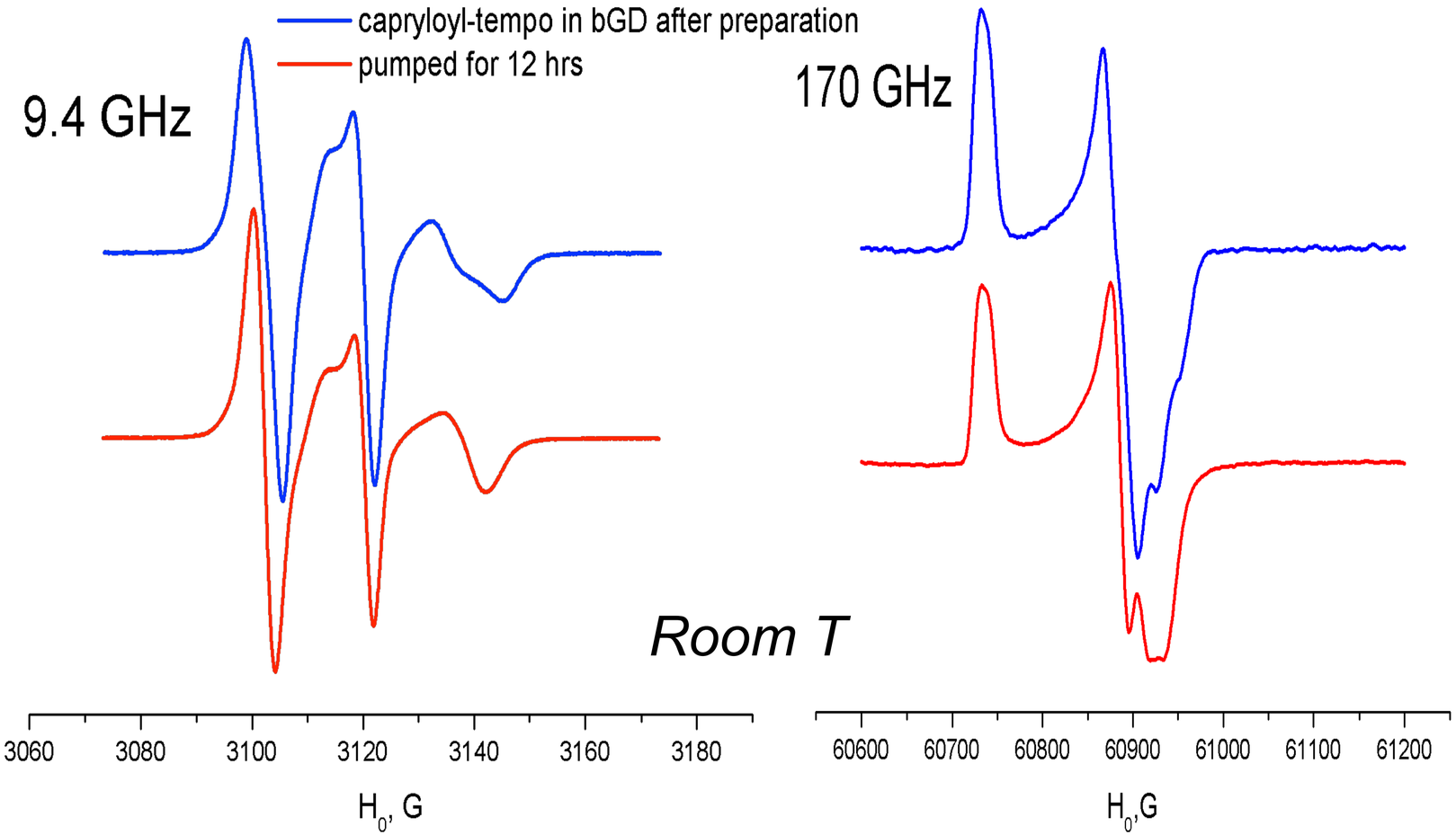

Diffusion tilt angle

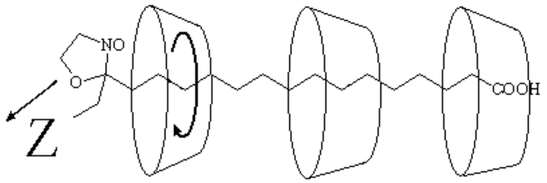

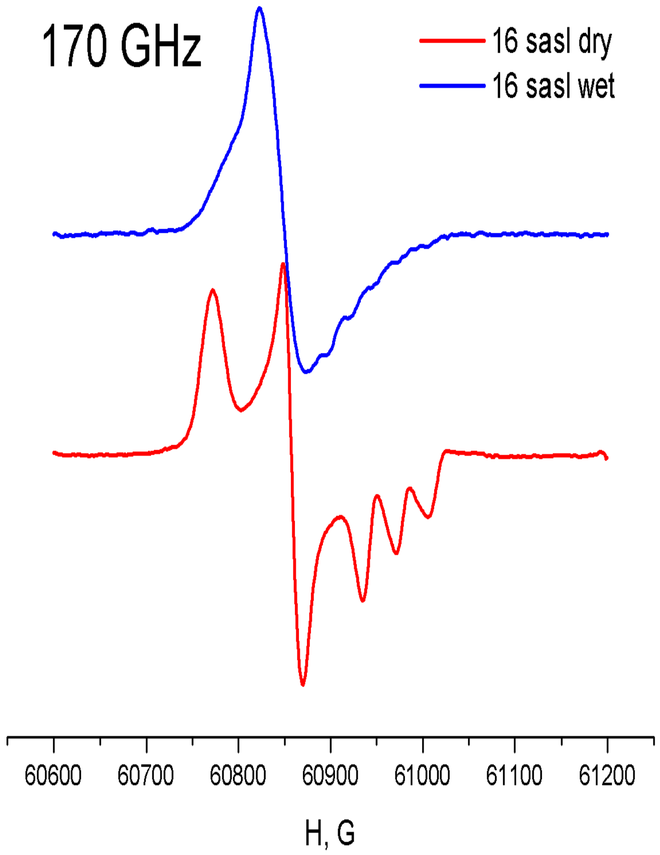

Y-rotation

Averaging *effective* tensor components

$(g_{xx}+ g_{zz})/2$, g_{yy}, $(g_{xx}+ g_{zz})/2$,
$(A_{xx}+ A_{zz})/2$, A_{yy}, $(A_{xx}+ A_{zz})/2$

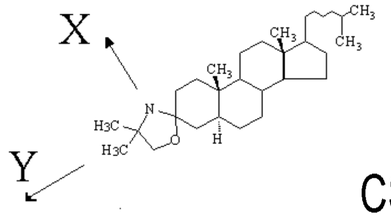

Room T

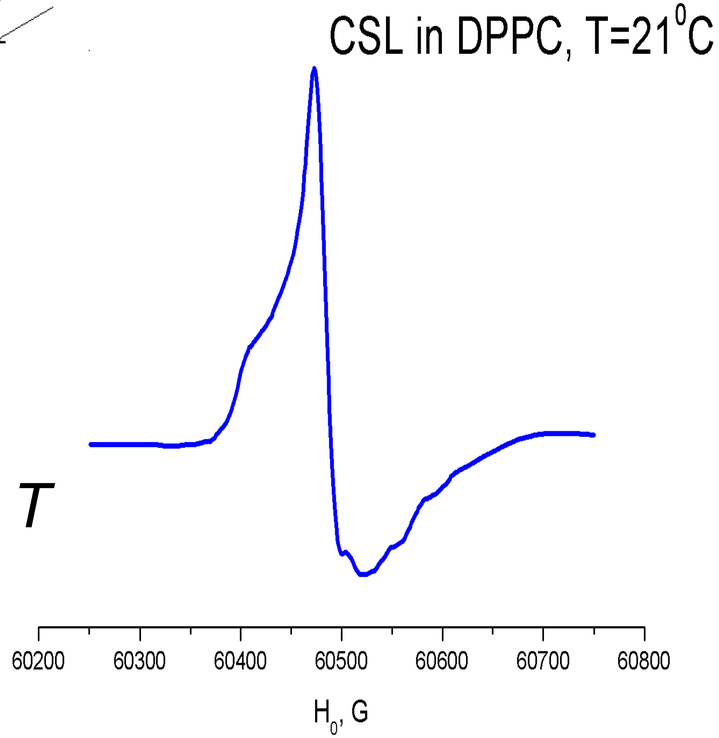

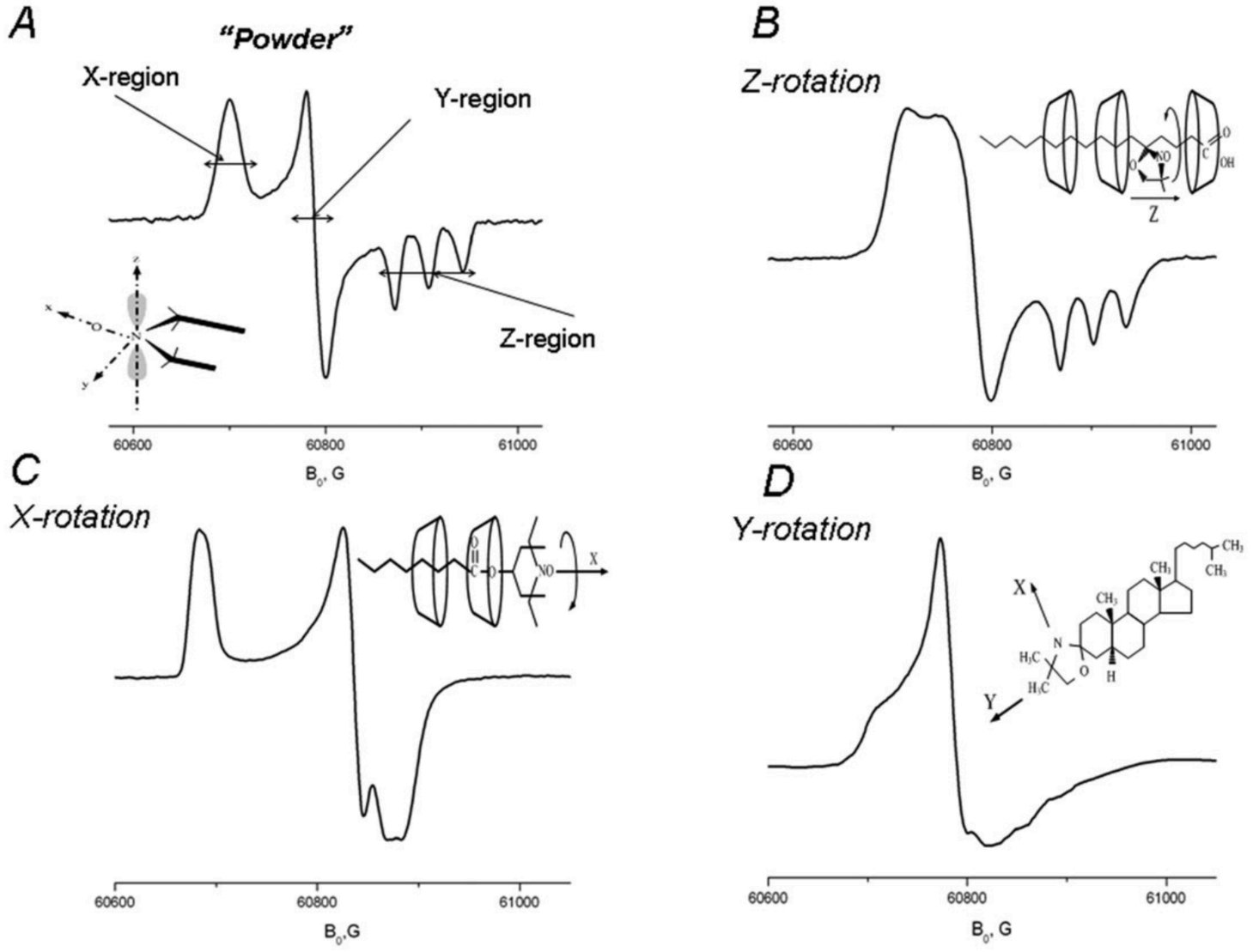

Fig. 3 170 GHz spectra of nitroxide radicals corresponding to different modes of molecular motion: (A) 5-sasl in γ-CD with crystallohydrate water removed by overnight evacuation at 293 K: rigid limit spectrum. (B) 5-sasl in γ-CD crystallohydrate at 292 K. (C) TEMPOyl-caprylate in β-CD at 293 K. (D) CSL spin label in the DPPC membrane at 295 K. Insert A shows the principal magnetic axes of the nitroxide group. Inserts B–D show the corresponding mode of molecular motion.

X-rotation

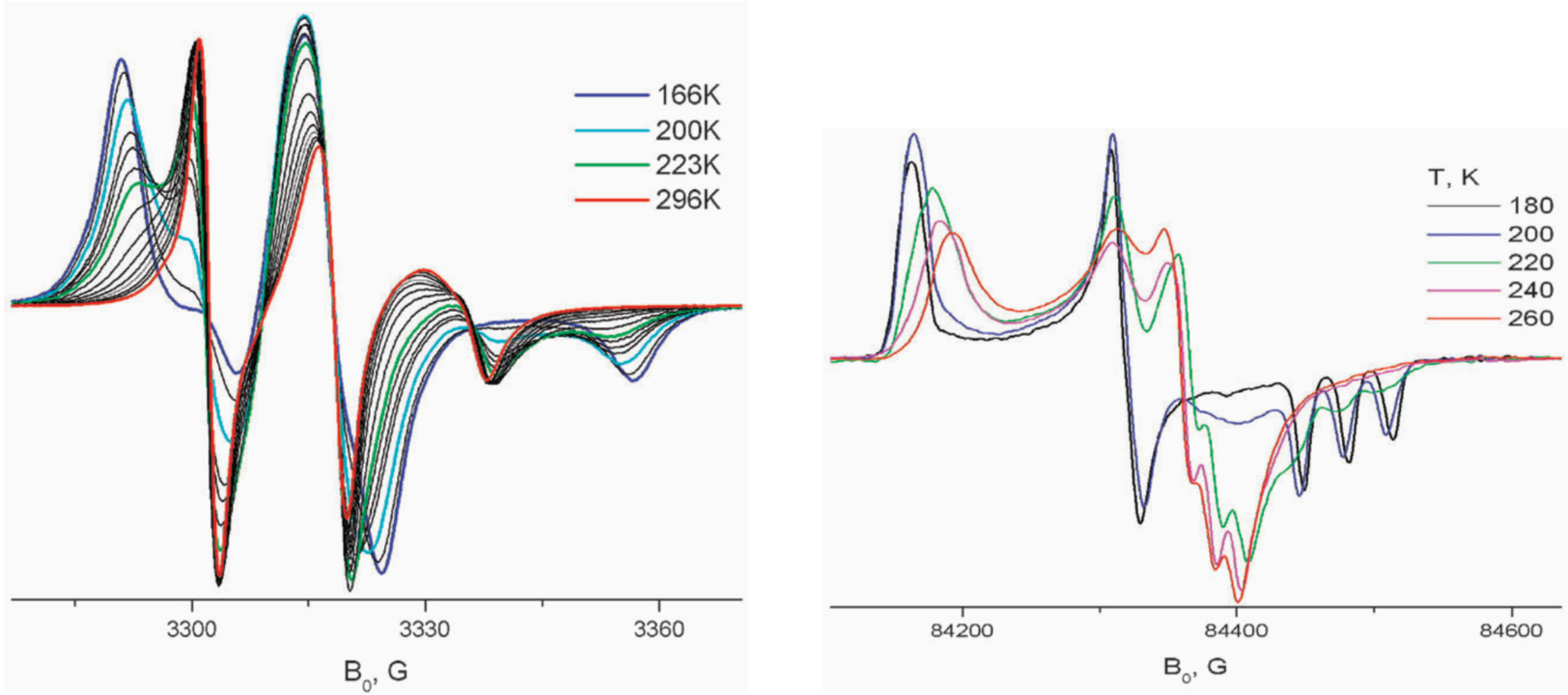

Fig. 15 TEMPOyl caprylate in γ-CD. Temperature dependence at 240 GHz (upper image) and 9 GHz (lower image).

*Dynamics **vs.** Dynamics + Orientational resolution*

ESR on aligned membranes

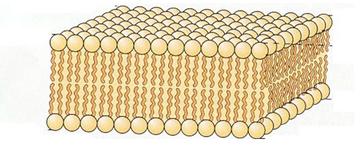

Spin-labeled gramicidin A in DPPC, 22⁰ C

Aligned membrane

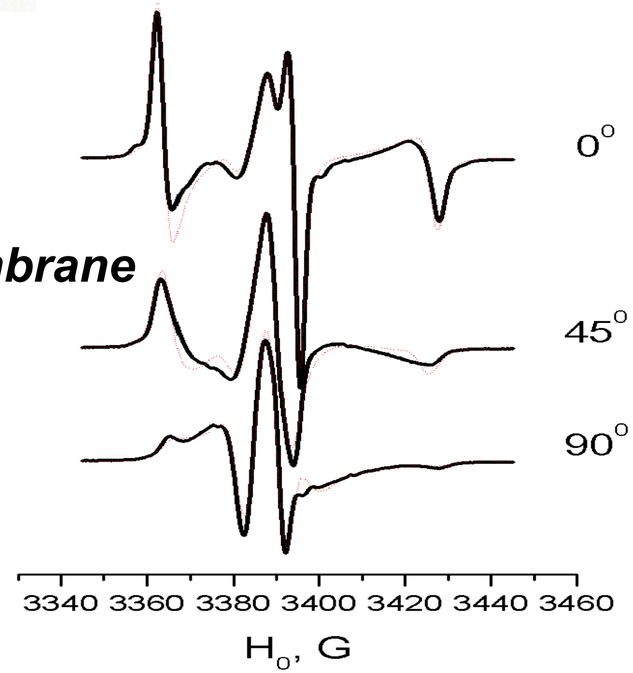

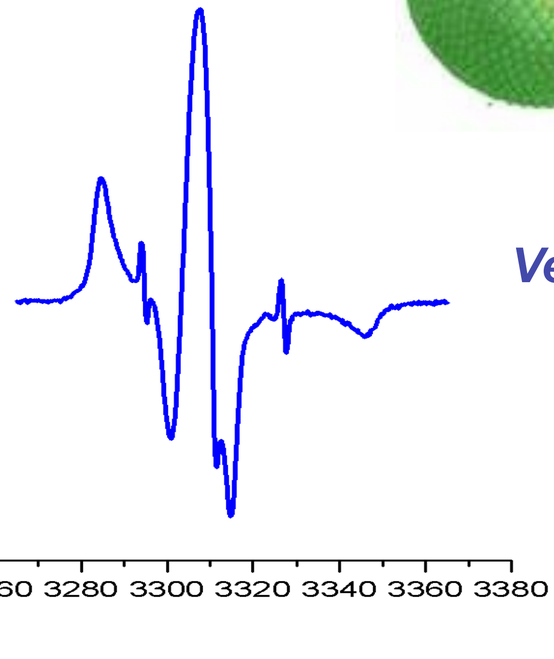

Vesicles

Simulation of angular dependent spectra is much freer of ambiguity, compared to vesicles

Application of aligned membranes allows extracting information on relative orientation of diffusion and magnetic axes, which can not be obtained from vesicles

Microtome technique on aligned membranes

High frequency ESR *requires very thin (<100 mm) flat samples with* B_0 *directed perpendicular to the sample in order to minimize dielectric losses*

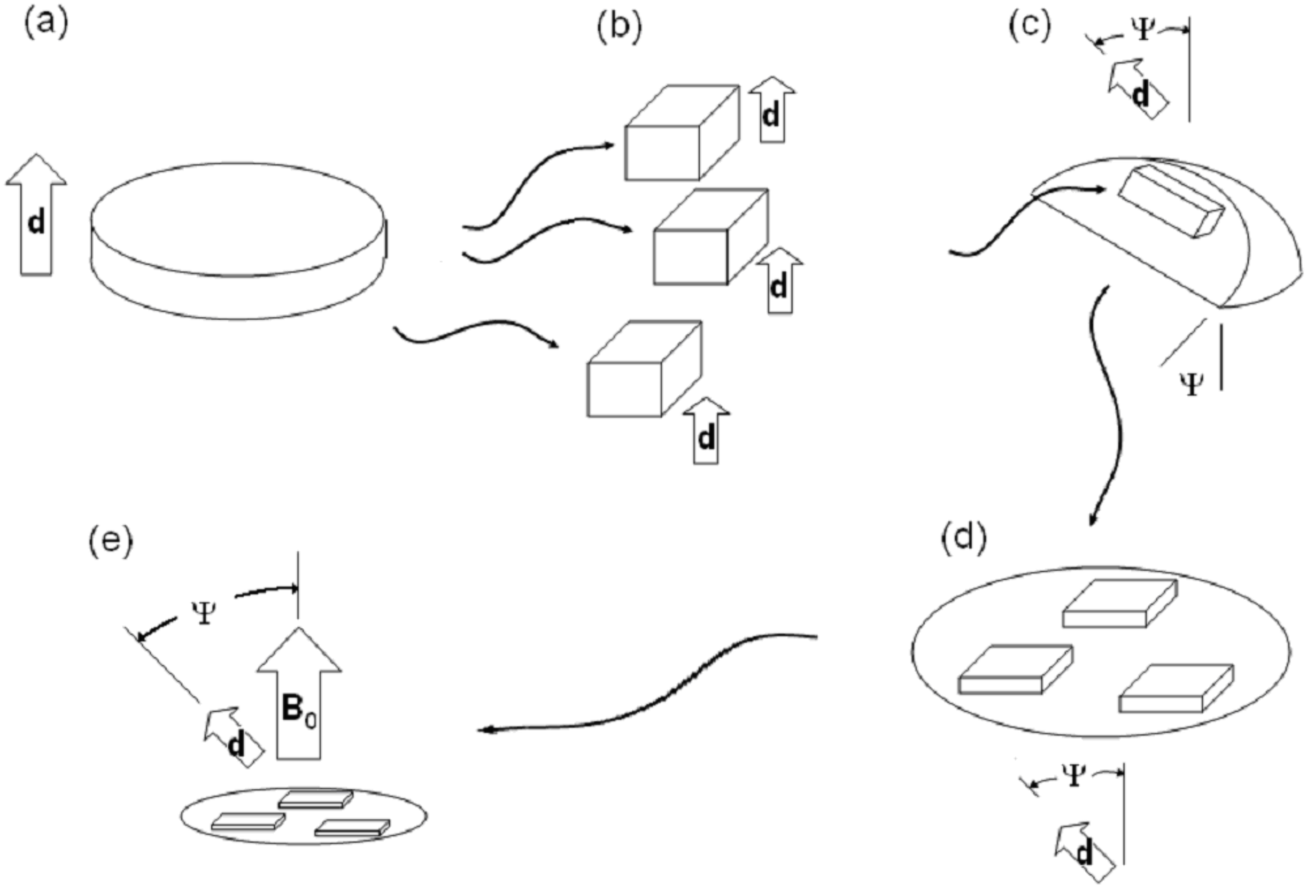

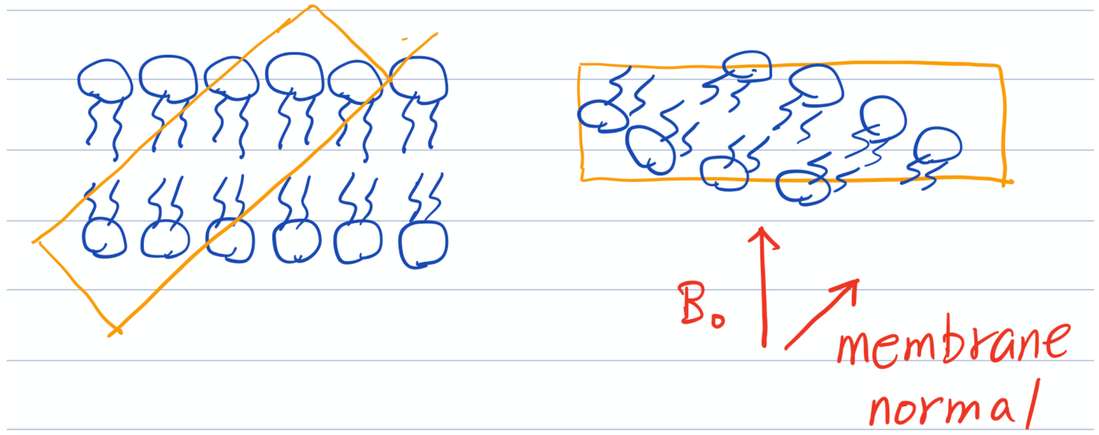

High-field ESR on aligned membranes

in different orientation of the membrane normal relative to B_o

ISDU aligned DPPC membrane sample is 300 micrometer think

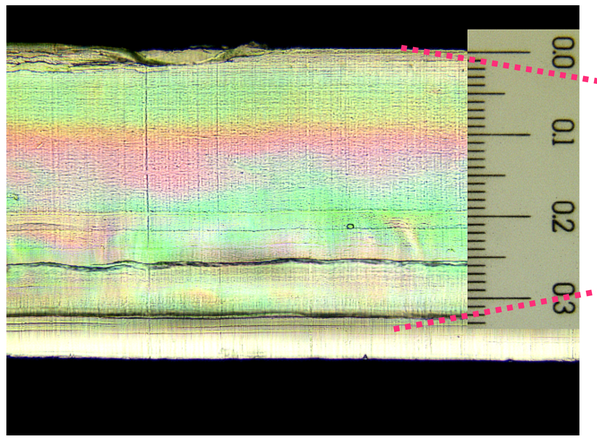

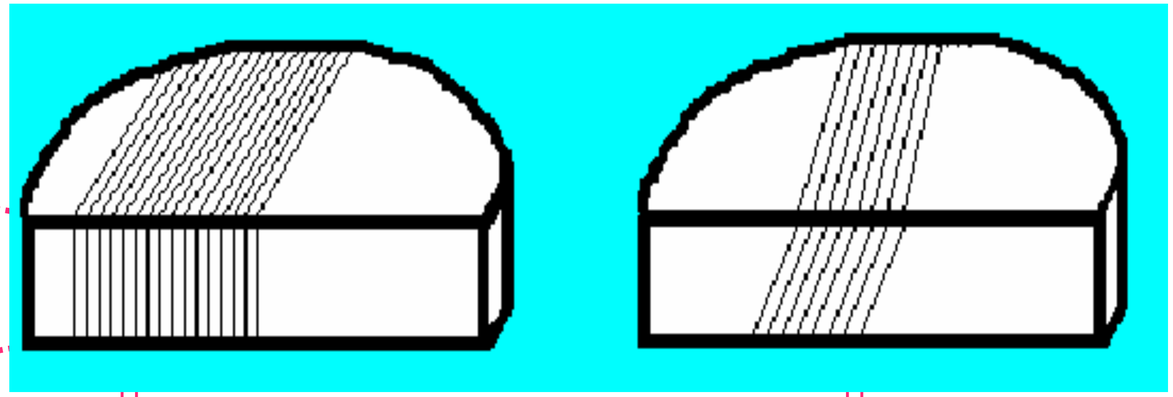

80micrometer slices cut of the sample

are utilized in high-field ESR

Spin labeled Gramicidin A in DPPC at 170 GHz

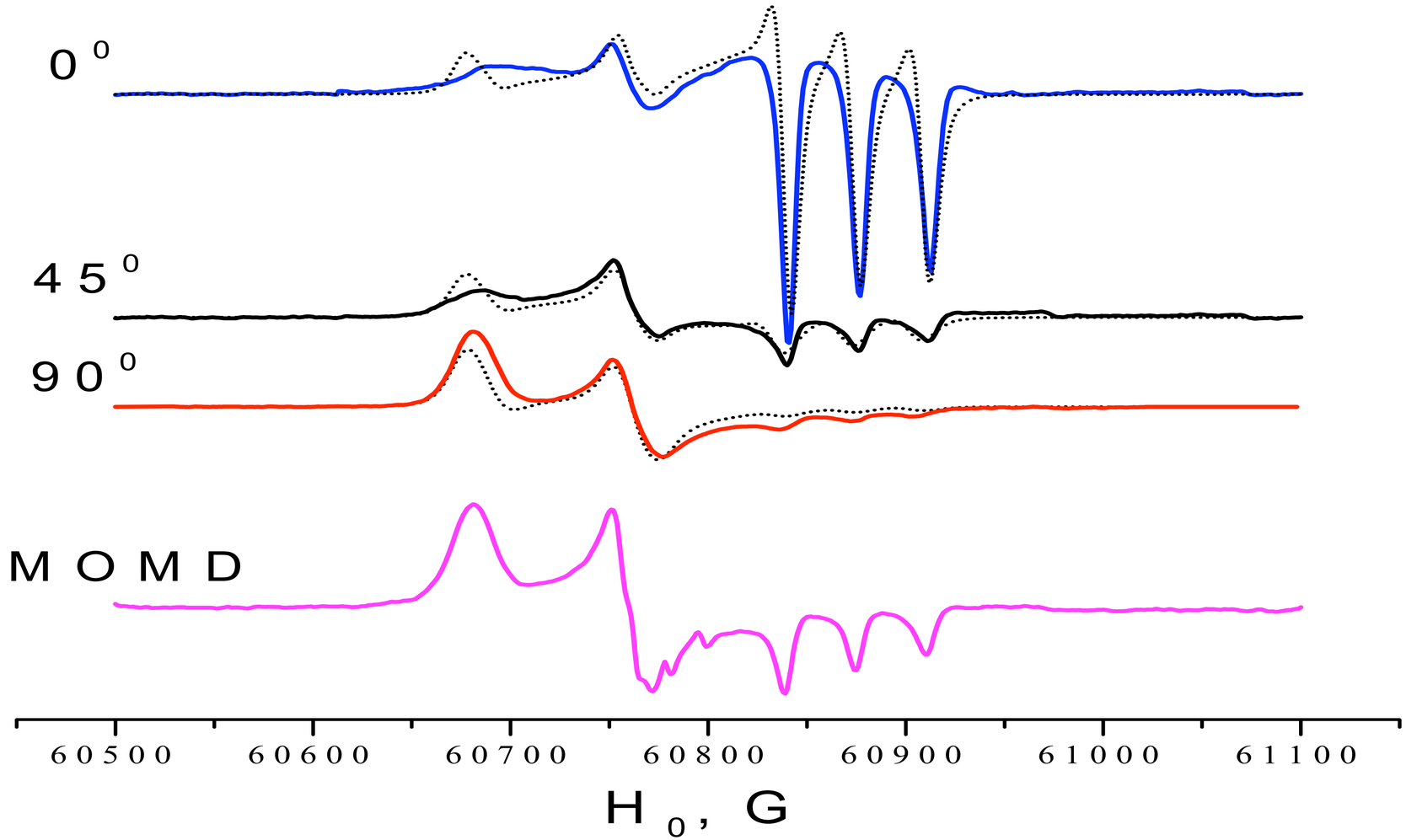

Spin-labeled Gramicidin A in Oriented Membrane (DPPC)

- *Slow motional nitroxyl spectrum at 7°C.*
- *Orientation selection at 95 GHz (3.2 mm)*
- *g_z parallel to membrane normal (z-ordered)*

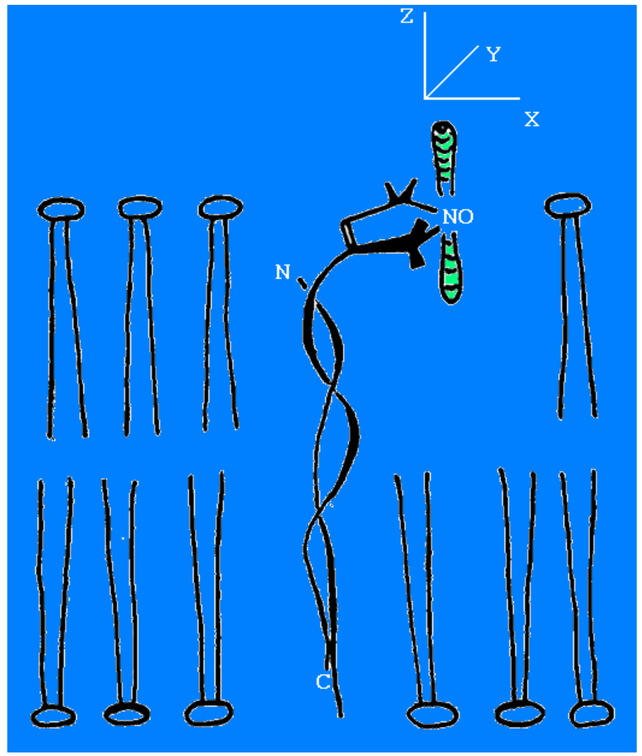

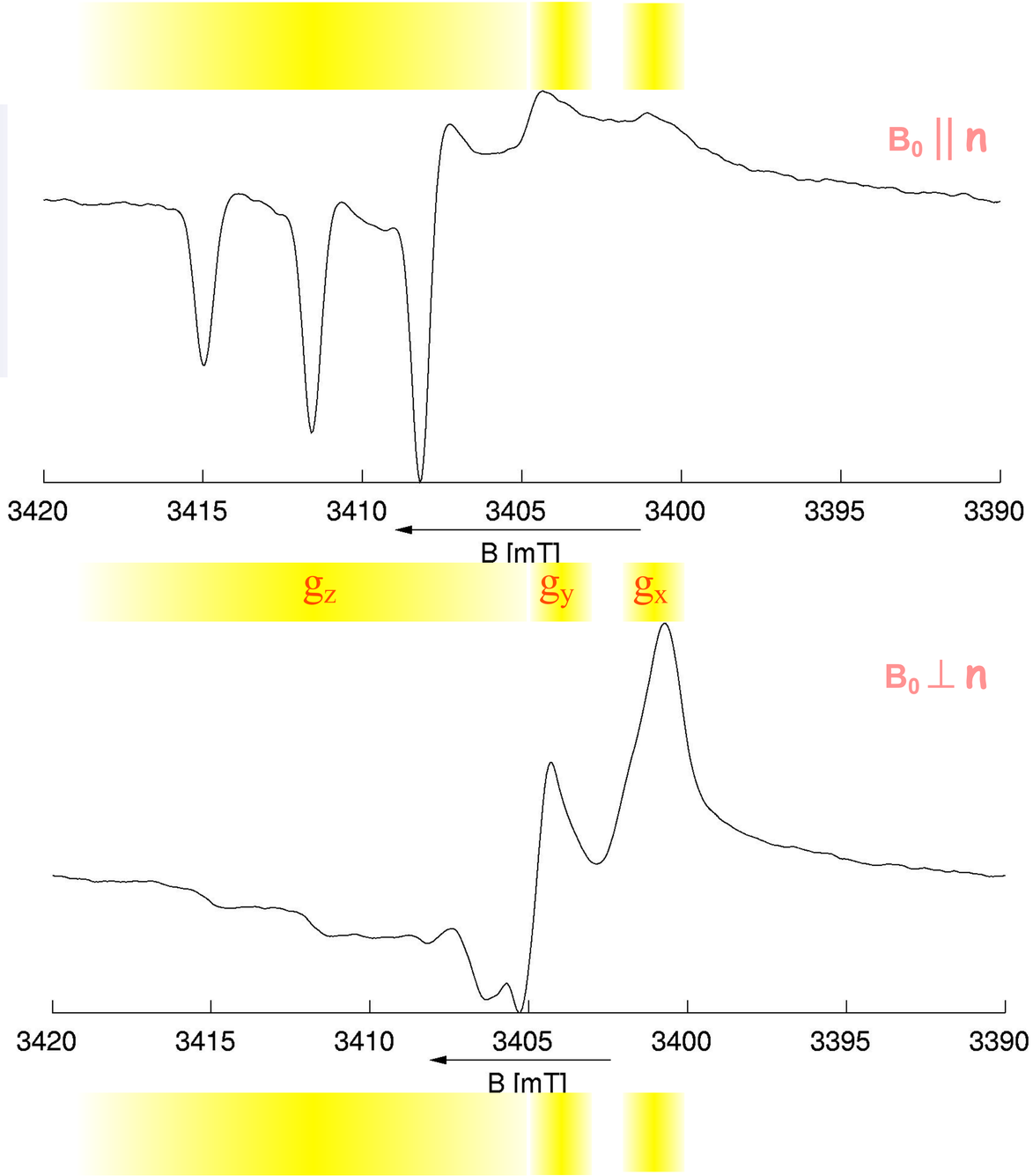

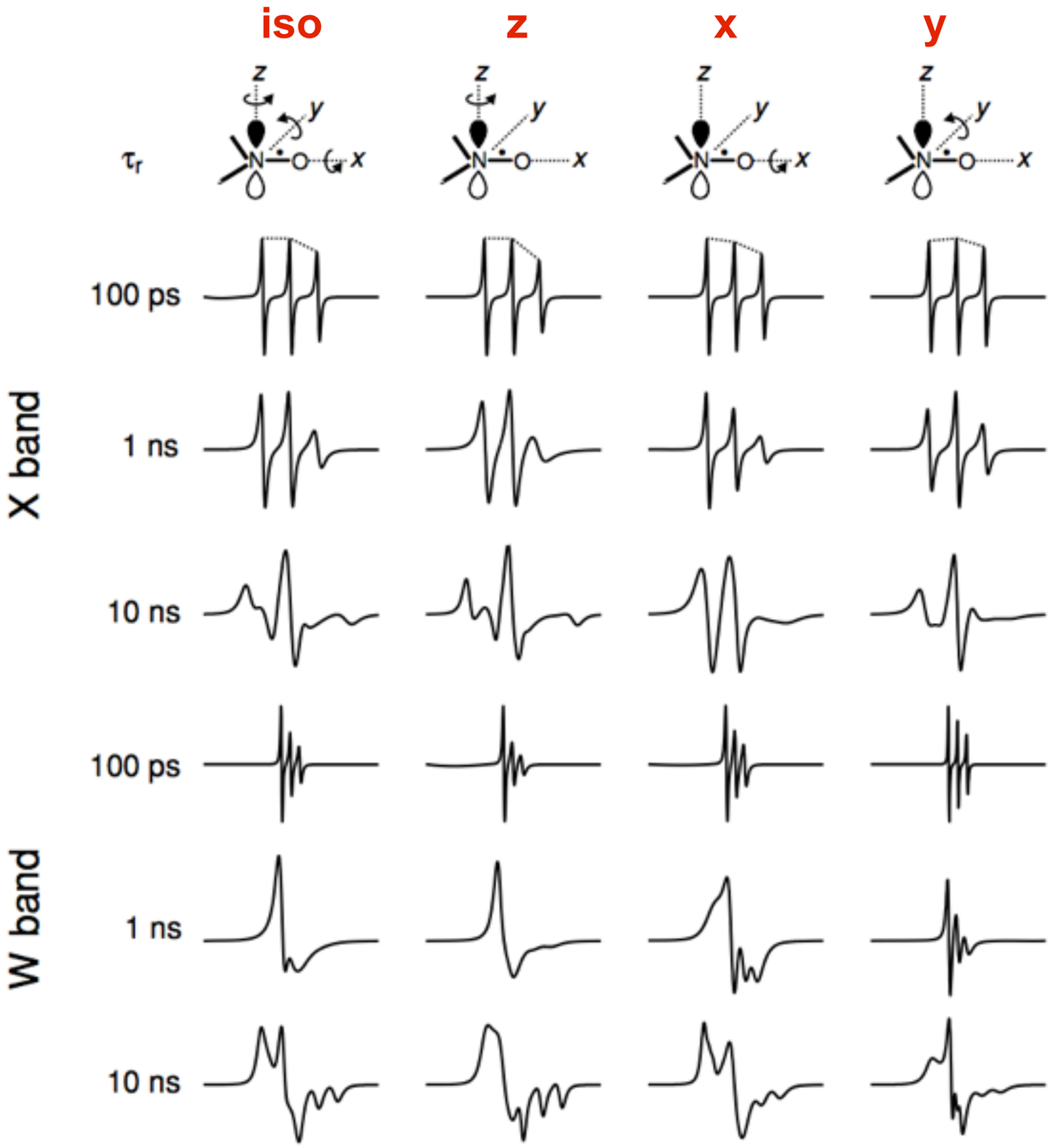

Fig. 1. Dependency of nitroxide spin probe spectra on rotational correlation time, preferential rotation axis, and EPR frequency. Panels from left to right correspond to isotropic rotational diffusion, and preferential rotation about the z, x, and y axis, respectively. Rotational diffusion about the preferred axis is assumed to be ten times faster than about other axes. X-band spectra are centered at 334.8 mT and are 10 mT wide, W-band spectra are centered at 3355 mT and are 30 mT wide. Simulations were performed with the Schneider/Freed suite of programs [21].

Lineshape depends on
1) diffusional rates (dynamics) 2) anisotropic rotations

Nano-confinement Enhances Anisotropic Rotational Dynamics ?

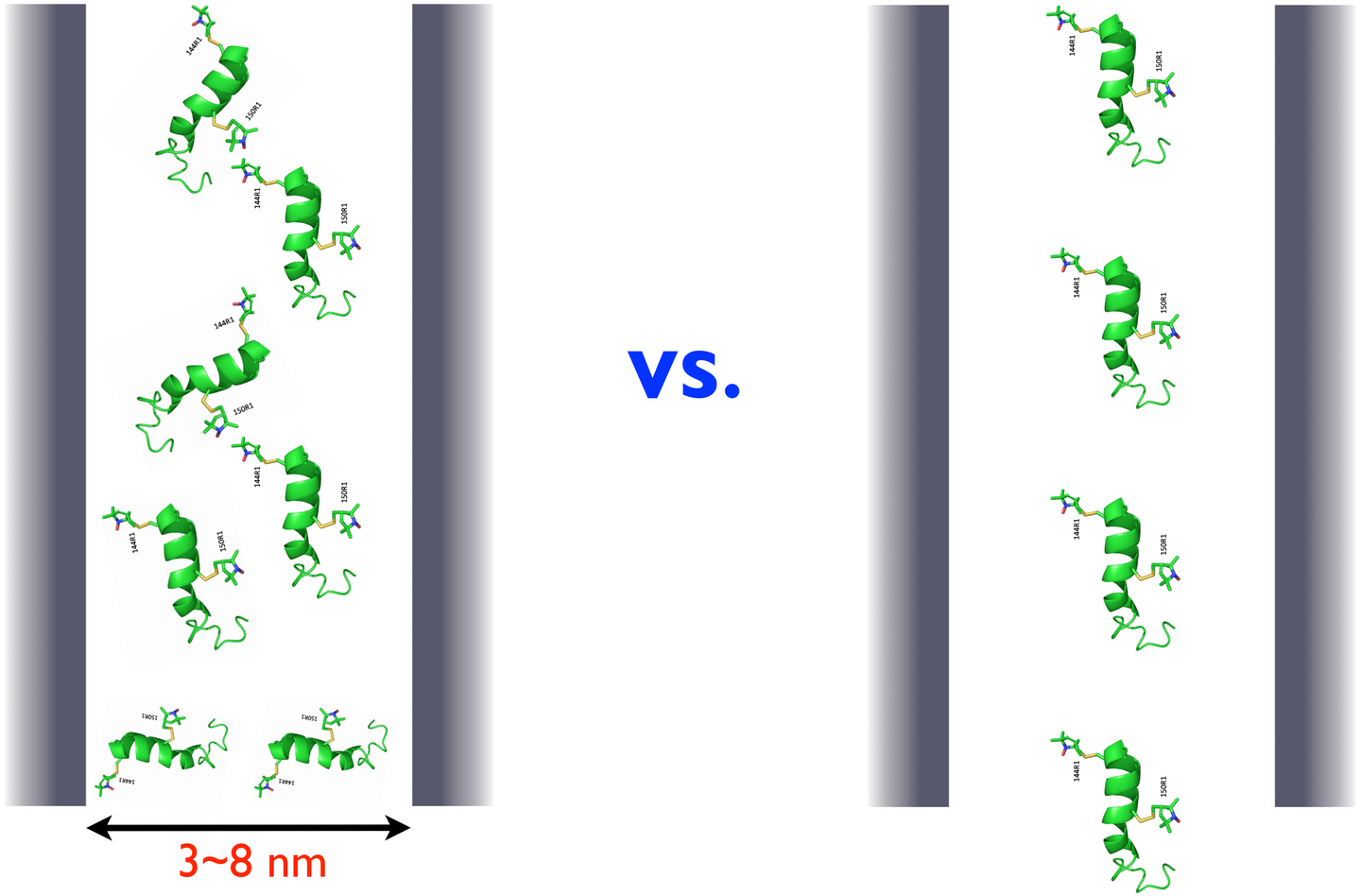

Is ESR useful for probing dynamics of a nanodevice confined deeply within nanostructures?

Peptide Retains its Structure in Nanochannels

PP-3R1 CPPPCPPPPPPPPC

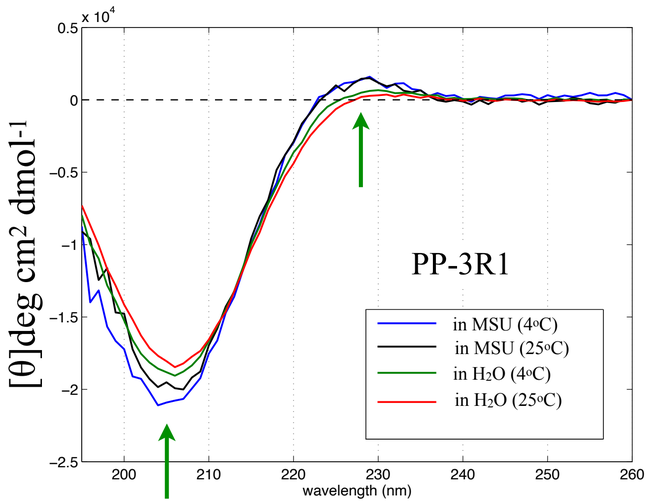

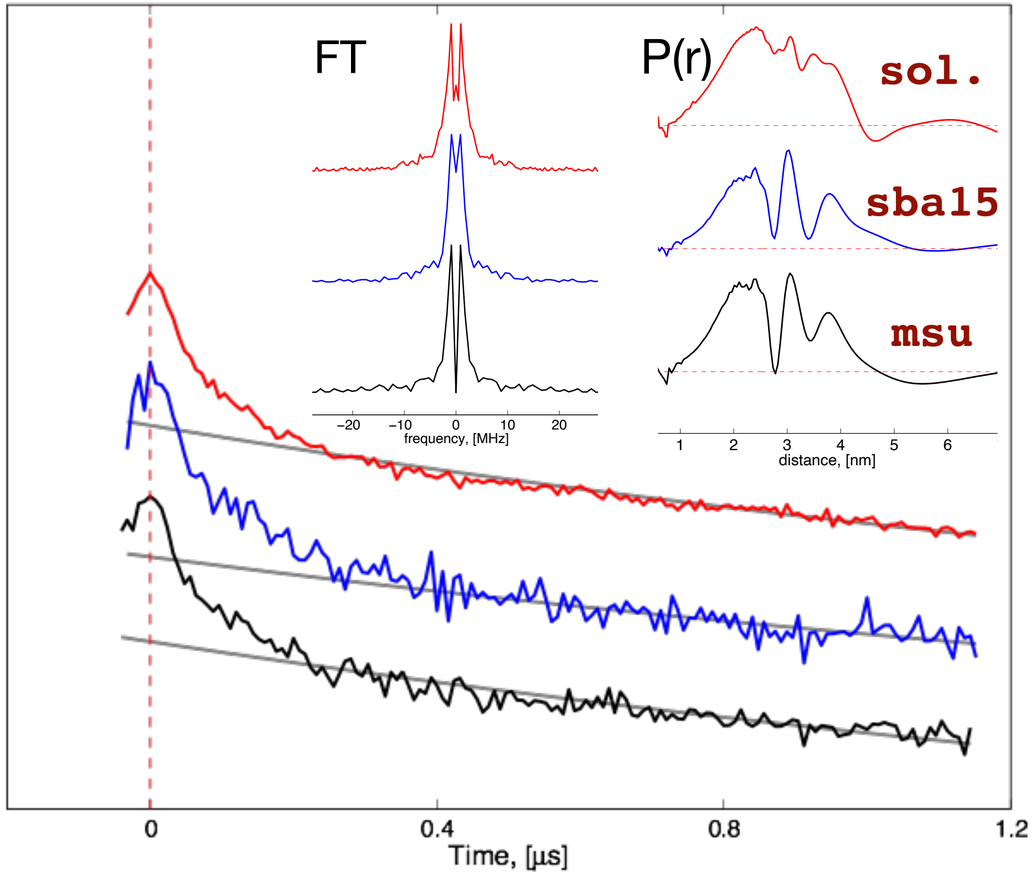

- CD shows PPII structure is unchanged.
- ESR demonstrates the peptide structure is approximately the same in all conditions studies.
- **P(r) accuracy improved.**

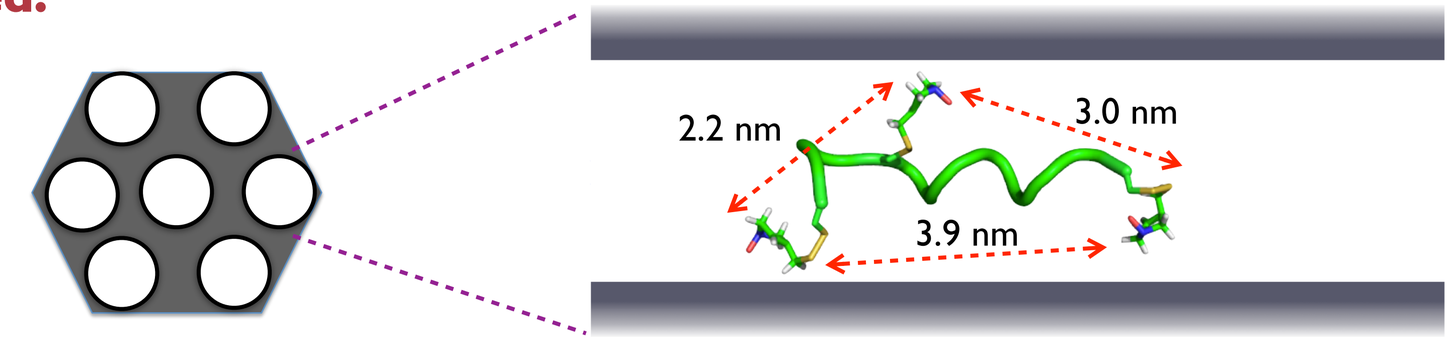

Theoretical Fits to Multifrequency Spectra

X-band (9 GHz)

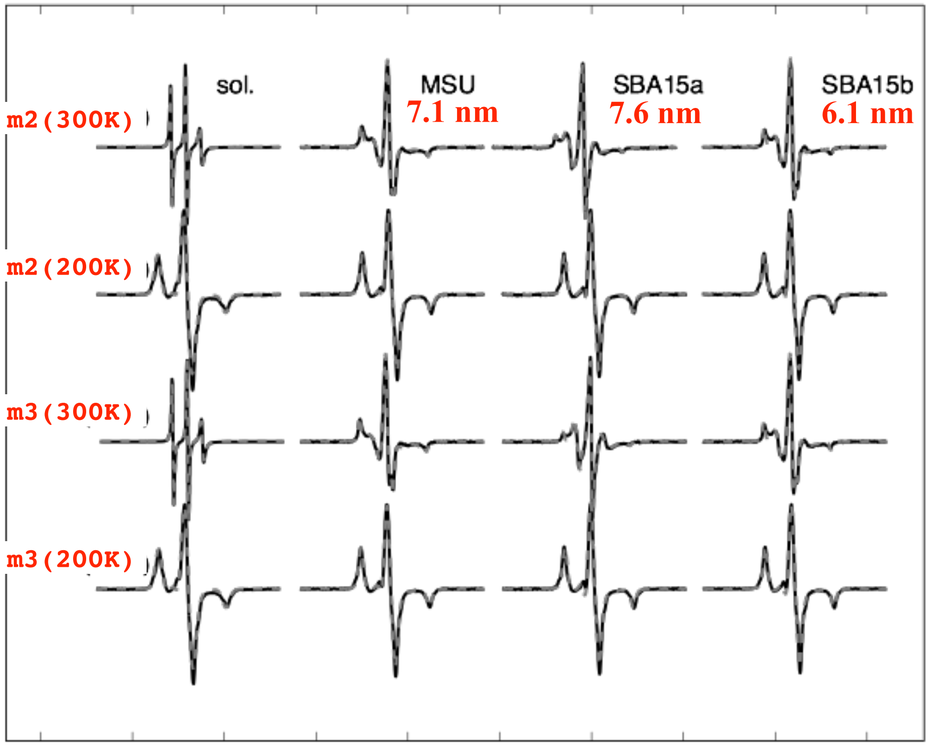

Q-band (35 GHz)

PP-m2 PPPPPPCPPPPPPP

PP-m3 PPPPPPPPCPPPPP

T = 300 K		$R_\perp$ (s^{-1})	$R_\parallel$ (s^{-1})	$R_\parallel/R_\perp$	S_0	$\Delta^{(0)a}$	[Im]^b
sol.		2.35×10^8	6.54×10^7	0.28	0.03	0.5	100% (100%)
MSU	Im	1.27×10^6	1.24×10^7	9.76	0.56	2.7	48% (38%)
	Mb	3.82×10^7	3.82×10^7	1.00	0.15	2.1	
SBA15a	Im	1.27×10^6	3.79×10^7	11.22	0.54	3.0	47% (32%)
	Mb	6.39×10^7	6.39×10^7	1.00	0.16	1.7	
SBA15b	Im	1.06×10^6	1.03×10^7	9.72	0.48	2.4	45% (46%)
	Mb	4.39×10^7	4.38×10^7	0.99	0.14	1.4	
T = 200 K	$R_\perp$ (s^{-1})	$R_\parallel$ (s^{-1})	$R_\parallel/R_\perp$	S_0	$\Delta^{(0)d}$	$\Delta^{(2)e}$	
sol.	6.81×10^5	1.71×10^5	0.25	0.62	7.5 (7.4)	0 (0)	
MSU	$(0.13 \pm 0.03) \times 10^6$	$(8.15 \pm 0.50) \times 10^6$	62.7	0.58 ± 0.05	1.9 (1.2)	4.6 (4.5)	
SBA15a	^{c}	^{c}	^{c}	^{c}	1.4 (1.6)	2.6 (3.3)	
SBA15b	^{c}	^{c}	^{c}	^{c}	1.4 (1.8)	3.9 (3.7)	

Multifrequency Analyses Unravel the Rotational Anisotropy

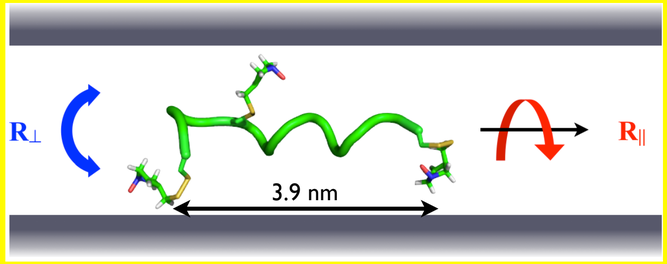

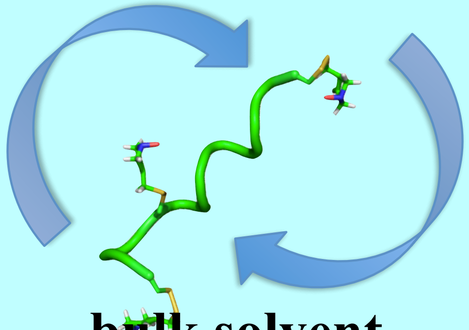

	Nanochannels (6, 7, 7,6 nm)	**bulk solvent**
$R_{\|\|}/R_{\perp}$	60 ← 10	0.26±0.02
S_0	0.54±0.04	0.62 ← 0.03
$\triangle^{(2)}$	3.6±1.0	~ 0
comp.	one ← two	one ← one
Temp	200 K, 300 K	200 K, 300 K

- Nano-confined molecules possess a greater **ordering** and anisotropy $R_{||}/R_{\perp}$ as compared to the bulk study.
- $R_{||}/R_{\perp}$ barely changes with pore sizes, as the nanoconfinement effects persist.

Significance of the Spectral Components

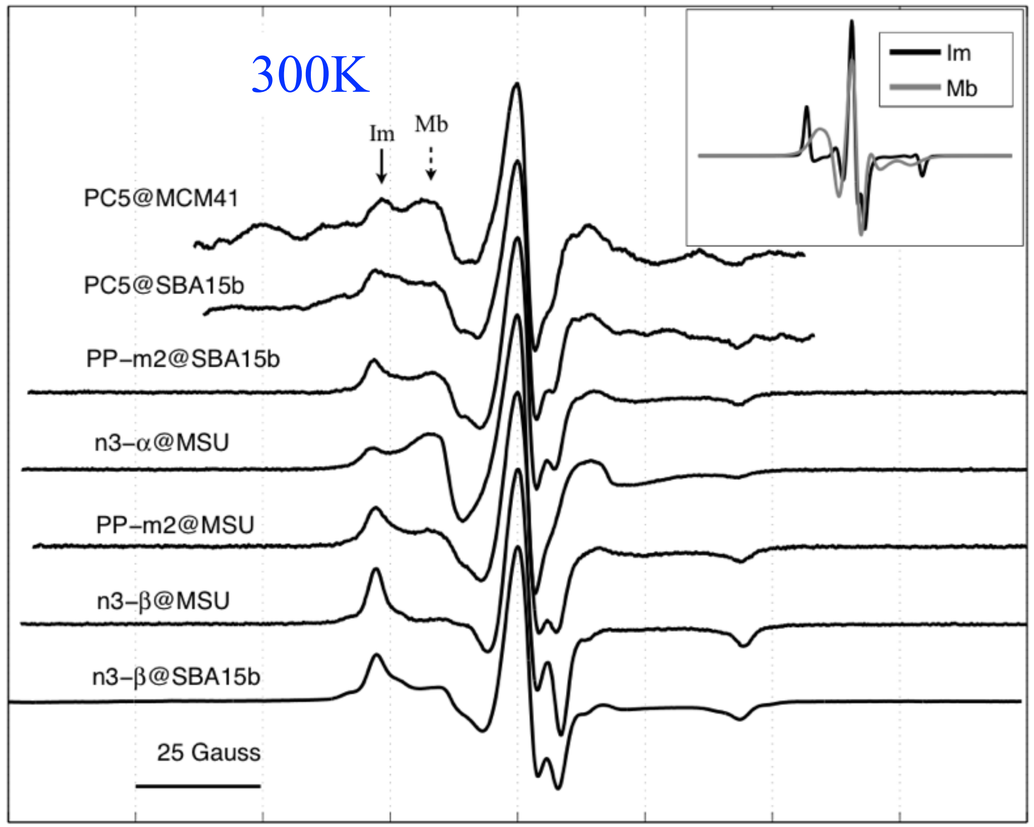

PC5

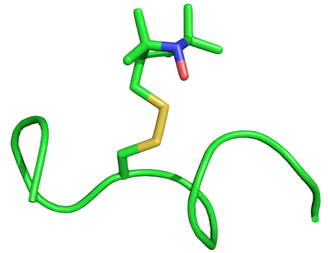

n3-α

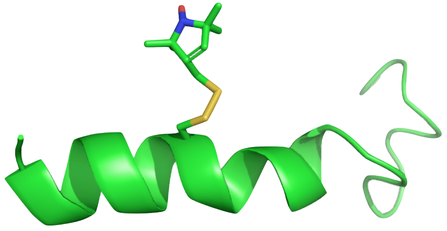

n3-β

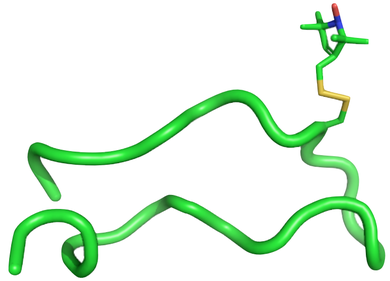

Mb reports

- *helical structural types (PPII or α-helix)* (X)
- *peptide length (11-, 14, or 26-aa long)* (X)
- *solvents (H_2O, PB, or TFE/PB)* (X)
- *pore sizes (2.5 ~7.6 nm)* (X)
- *backbone dynamics on secondary structures (helix vs. hairpin)* (O)

JACS
JOURNAL OF THE AMERICAN CHEMICAL SOCIETY
Cite This: J. Am. Chem. Soc. 2018, 140, 16032−16036
Commur
pubs.acs.

How Do Enzymes Orient When Trapped on Metal−Organic Framework (MOF) Surfaces?

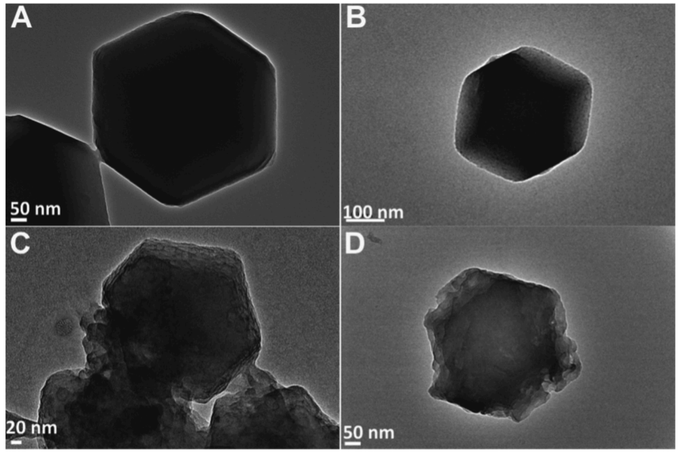

Figure 1. TEM images of ZIF-8 in MeOH (A) and PBS buffer (B) and hL/ZIF-8 composites in MeOH (C) and PBS buffer (D).

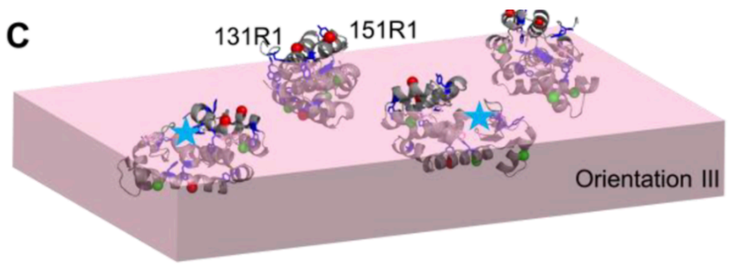

Red: residues more likely to be buried (72R1, 131R1, and 151R1);
Green: residues more likely to be exposed (44R1, 65R1, and 118R1);
Blue sticks: exposed aromatic residues;
Star: T4L active site; pink: ZIF-8 scaffold.

Figure 4. Proposed orientations of T4L on ZIF-8 crystal surface from four angles differing by 90° clockwise. For details of model construction and other possible orientations, see the SI.

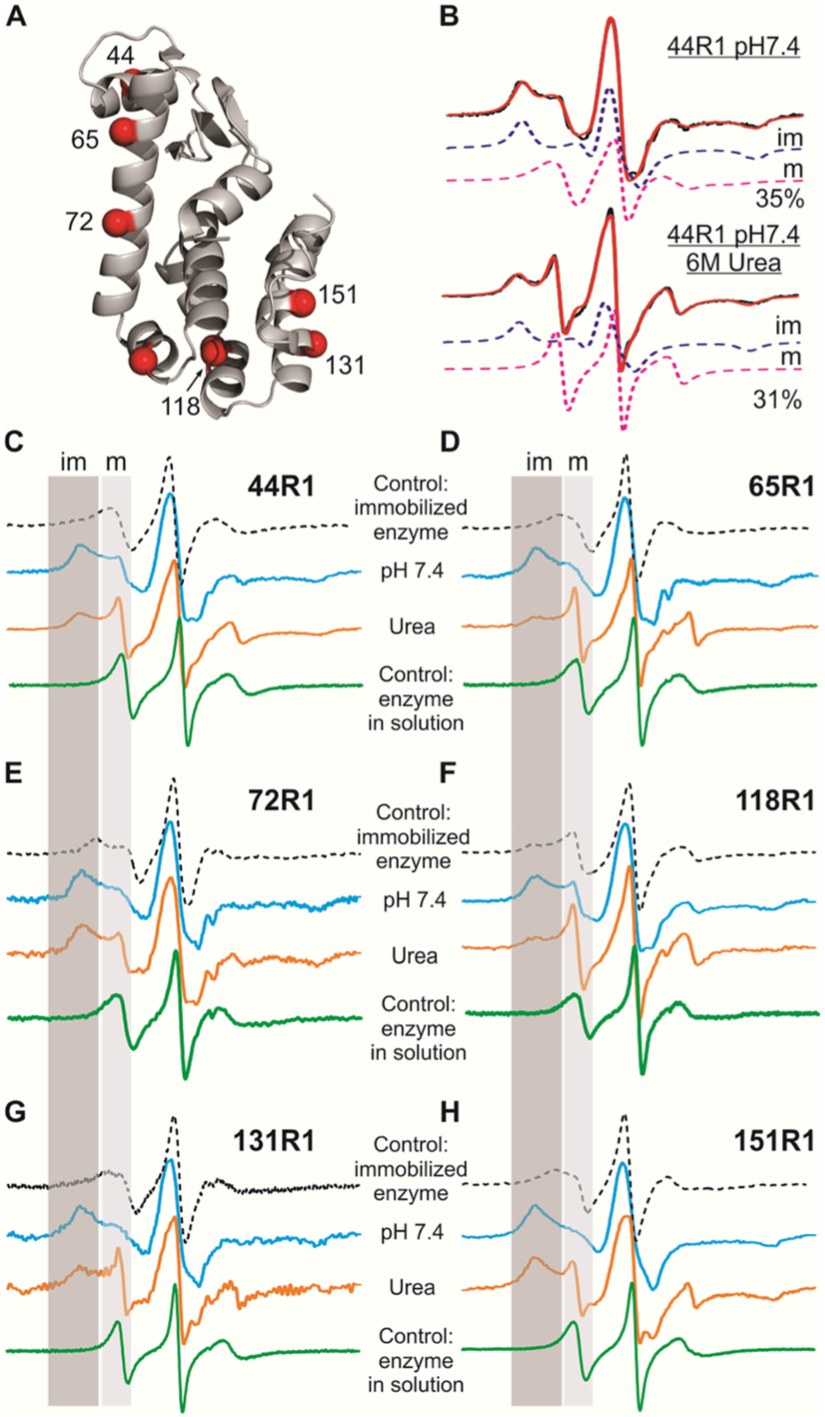

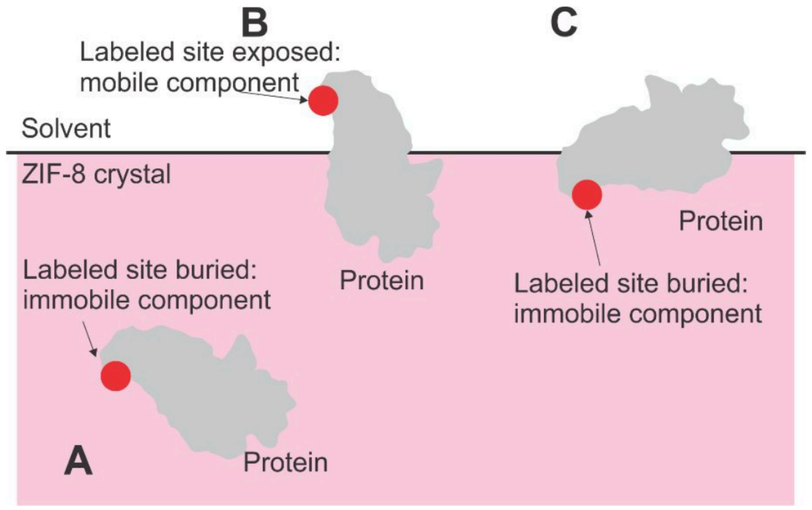

immobilized/trapped in MOFs due to the interferences of the MOF background signals. To address such challenge, we demonstrate in this work the utilization of site-directed spin labeling in combination with Electron Paramagnetic Resonance spectroscopy, which allows for the first time the characterization of the orientation of enzymes trapped on MOF surfaces. The obtained insights are fundamentally important for MOF-based enzyme immobilization design and understanding enzyme orientation once

Figure S6. Schematic illustration of EPR signal reporting both buried and solvent-exposed enzymes. Buried sites, either buried deep inside (A) or partially buried below the crystal surface (C) will contribute an immobile component to the EPR spectrum, while an exposed labeled site (B) will show a mobile component in the spectrum.

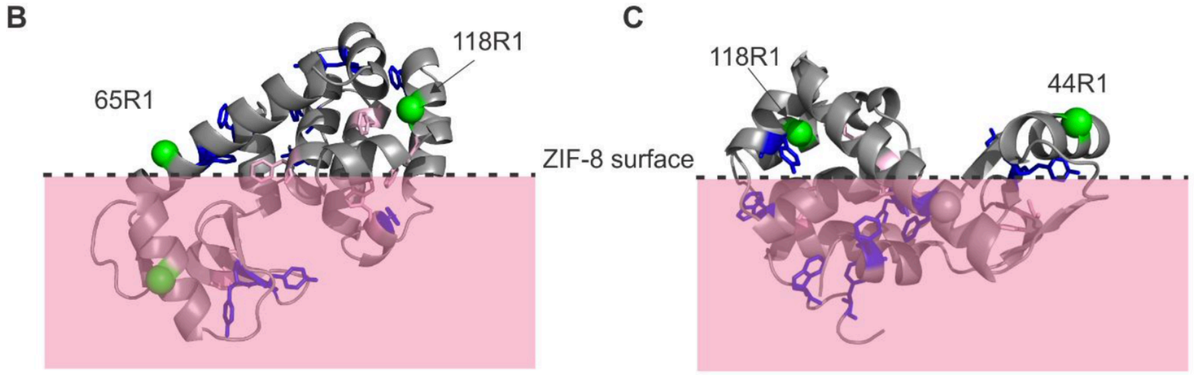

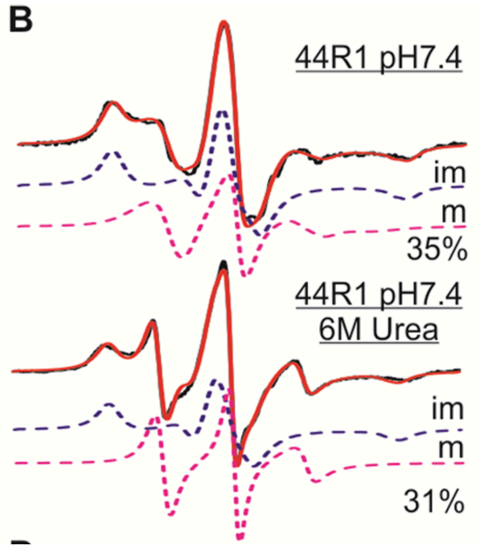

Figure S9. (A) An orientation to expose 44R1, 65R1, and 118R1 simultaneously. The buried portion (below the dotted line) is likely too small to trap the enzyme under the ZIF-8 crystal surface. (B) An orientation to expose 65R1 and 118R1. The buried portion is also too small to trap the enzyme under the ZIF-8 crystal surface. (C) It might be possible to simultaneously expose 44R1 and 118R because the buried portion is dominant.